NATIONAL ENERGY TECHNOLOGY LABORATORY

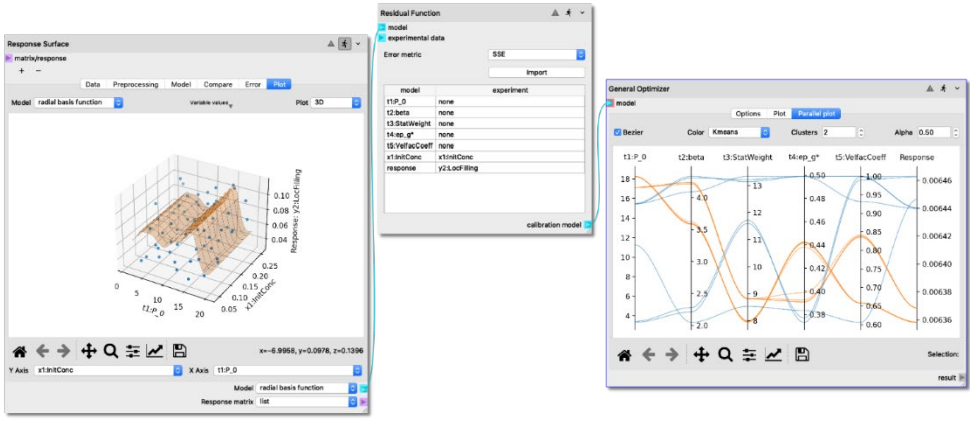

Deterministic Calibration of MFiX-PIC, Part 1: Settling Bed

10 February 2021

U.S. DEPARTMENT OF ENERGY | NATIONAL ENERGY TECHNOLOGY LABORATORY

Office of Fossil Energy

DOE/NETL-2021/2646

Disclaimer

This work was funded by the Department of Energy, National Energy Technology Laboratory, an agency of the United States Government, through a support contract with Leidos Research Support Team (LRST).

Cover Illustration: Screenshot of the workflow setup in Nodeworks UQ software developed by NETL for demonstration of the deterministic calibration of the particle settling bed application, which employs a surrogate model to characterize the relationship between six input parameters and the quantity of interest (QoI) for the given simulation campaign dataset. A residual function node that computes the residual error between surrogate model-based simulation results and analytical solution, which is used with the general optimizer node to find the best settings for the five model parameters being calibrated that yields to lowest residual error.

Suggested Citation: Gel, A.; Vaidheeswaran, A.; Clarke M. A. *Deterministic Calibration of MFiX-PIC, Part 1: Settling Bed*; DOE.NETL-2021.2646; NETL Technical Report Series; U.S. Department of Energy, National Energy Technology Laboratory: Morgantown, WV, 2021; p 72. DOI: 10.2172/1764832.

An electronic version of this report can be found at:

Technical Reports Series (TRS) | netl.doe.gov

Deterministic Calibration of MFiX-PIC, Part 1: Settling Bed

Aytekin Gel[1,2], Avinash Vaidheeswaran[1], Mary Ann Clarke[1]

[1] **U.S. Department of Energy, National Energy Technology Laboratory, Leidos Research Support Team, 3610 Collins Ferry Road, Morgantown, WV 26507**

[2] **U.S. Department of Energy, National Energy Technology Laboratory, ALPEMI Consulting, L.L.C., 3610 Collins Ferry Road, Morgantown, WV 26507**

DOE/NETL-2021/2646

10 February 2021

NETL Contacts:

Jeff Dietiker, Mehrdad Shahnam, William Rogers, Co-Principal Investigators

William A. Rogers, Technical Portfolio Lead

Bryan Morreale, Executive Director, Research & Innovation Center

This page intentionally left blank.

Table of Contents

List of Figures

List of Figures (cont.)

List of Tables

Acronyms and Abbreviations

Term	Description
ASCII	American Standard Code for Information Interchange
BOBYQA	Bound Optimization By Quadratic Approximation
CFD	Computational fluid dynamics
DEM	Discrete element method
DOE	Design of experiments
GO	General optimizer
HPC	High performance computing
LGPL	Lesser General Public License
LH	Latin Hypercube
MARS	Multivariate Adaptive Regression Splines
MCMC	Markov Chain Monte Carlo
MFiX	Multiphase Flow with Interphase eXchanges
MFiX-DEM	MFiX discrete element method solver
MFiX-PIC	MFiX particle-in-cell solver
MFiX-TFM	MFiX two-fluid model solver
OLH	Optimal Latin Hypercube
PIC	Particle-in-cell
RMSE	Root mean square error
RS	Response surface
QoI	Quantities of Interest (a.k.a. response variable)
SBE	Simulation-based engineering
TFM	Two-fluid model

List of Symbols

Symbol	Description
R^2 or R-squared	Goodness-of-fit measure for linear regression models
θ_1 or Theta1 or t1:P_0	Pressure linear scale factor, (P_0)
θ_2 or Theta2 or t2:beta	Volume fraction exponential scale factor, (β)
θ_3 or Theta3 or t3:StatWeight	Statistical Weight (W_p)
θ_4 or Theta4 or t4:ep_g*	Void fraction at maximal close packing, (ϵ_g^*)
θ_5 or Theta5 or t5:VelfacCoeff	Solids slip velocity scale factor (α)
x_1 or x1	Initial solids concentration (ϵ_{s0})
y_1 or y1	Location of Settling Shock (mm)
y_2 or y2	Location of Filling Front or Shock (mm)
y_3 or y3	Void fraction at the first cell
m_p	Particle mass
U_i	Parcel velocity in coordinate direction i
ϵ_g	Gas volume fraction
ϵ_g^*	Gas volume fraction at solids close pack
ϵ_{g0}	Initial gas volume fraction
ρ_s	Solids density
ϵ_s	Solids volume fraction
ϵ_s^*	Solids volume fraction at close pack
ϵ_{s0}	Initial solids volume fraction
τ_p	Interparticle solids stress
$S_{mi,drag}^{(p)}$	Source term for drag
P_g	Fluid phase pressure
U_{gi}	Fluid phase velocity in coordinate direction i
$\beta_g^{(p)}$	p^{th} parcel's drag coefficient
δ	Very small number like 1E-7

List of Symbols (cont.)

Symbol	Description
δu_p	Estimated discrete particle velocity contribution
u_{r0}	Relative velocity at initial conditions
u_r^*	Relative velocity at solids close pack conditions
t	Time
W_p,	Statistical weight

Due to font constraints in plotting software, alternate abbreviated forms of the symbols were used for parameters and quantities of interest as shown in the above List of Symbols.

Acknowledgments

This work was performed in support of the U.S. Department of Energy's (DOE) Fossil Energy Crosscutting Technology Research Program. The research was executed through the National Energy Technology Laboratory's (NETL) Research and Innovation Center's CFD for Advanced Reactor Design (CARD) Field Work Proposal. Research performed by Leidos Research Support Team staff was conducted under the RSS contract 89243318CFE000003.

The authors wish to acknowledge Dr. William A. Rogers for programmatic guidance, direction, and strong support to carry out this research. The authors would like to thank Mr. Justin Weber of NETL for his keen support in addressing inquiries regarding Nodeworks, and also for quickly adding the desired features or nodes to Nodeworks, which enable the software to perform deterministic calibration. The authors also would like to thank Dr. Charles Tong of Lawrence Livermore National Laboratory for the support he provided in using PSUADE, including enabling PSUADE to perform a deterministic calibration workflow by modifying the exported surrogate model. Finally, the authors would like to acknowledge and thank Dr. Jean-François Dietiker for the suggestion to explore hybrid combination of settings as listed in Table 3.

EXECUTIVE SUMMARY

The Particle-in-cell (PIC) numerical approach for modeling granular solids in fluid flow has gained significant interest in recent years. Valued for its often shorter time-to-solution, the PIC formulation relies on modeling statistical groupings of particles called *parcels* in cooperation with a solids stress model to affect local solids velocity. This is in contrast to the discrete element model (DEM) where every particle in a system is modelled individually and directly coupled to local solids velocity through Newtonian mechanics.

The U.S. Department of Energy (DOE), National Energy Technology Laboratory (NETL) develops and maintains Multiphase Flow with Interphase eXchanges (MFiX), a collection of open-source computational fluid dynamics (CFD) solvers. Included in the MFiX suite are traditional two-fluid model (TFM) and DEM solvers, and a recently added PIC solver (NETL, 2021). In general, PIC methodologies offer an accuracy trade-off in lieu of computational speed; and therefore, it is important to assess the credibility of MFiX-PIC simulations. For this purpose, a systematic verification, validation and uncertainty quantification (VVUQ) effort was initiated at NETL to assess the new PIC solver.

This manuscript follows two earlier reports related to (1) verification and validation (V&V) of MFiX-PIC (Vaidheeswaran et al., 2020) and (2) sensitivity analysis of MFiX-PIC (Vaidheeswaran et al., 2021). The first study aimed to capture and document any discrepancy noted in MFiX-PIC by comparing simulation results to available experimental data directly. The second study aimed to create a better understanding of keyword-accessible modeling parameters employed in MFiX-PIC, by examining several quantities of interest (QoI) as the modeling parameters varied to determine their sensitivities. The current study aims to systematically document how to assess appropriate settings for MFiX-PIC keyword-accessible modeling parameters so that the least discrepancy is observed between MFiX-PIC simulation predictions and experimental results for a targeted application. Specifically, this technical report documents the process of calibrating multiple MFiX-PIC modeling parameters based on matching either an experimental dataset or an analytic solution. For this purpose, three application problems were selected: (1) particle settling, (2) fluidized bed, and (3) circulating fluidized bed. These problems purposefully span a wide selection of flow regimes with the expectation that a user may utilize similar MFiX-PIC modeling parameters for other related applications.

Calibration methodologies are usually grouped under two categories: (1) deterministic calibration, which provides a single value of each model parameter calibrated; and (2) statistical calibration, which provides a distribution for each model parameter calibrated based on insight provided by experimental data. As part of the deterministic calibration demonstration, two uncertainty quantification (UQ) software tools were employed to assess ease of use and to compare the performance of the proposed calibrated model parameter settings from each tool. UQ software tools included PSUADE and Nodeworks.

This report documents deterministic calibration of five MFiX-PIC modeling parameters in the context of particle settling. Simulation results are compared to an analytical solution for the location of the filling shock in a settling bed to assess the effectiveness of the proposed calibrated model parameter settings, which were determined to be quite different than the default MFiX-PIC settings and those proposed in the earlier V&V Manual. The observed difference was anywhere between 145% higher and 85% lower than the reference settings when compared. The proposed calibrated model parameter settings were demonstrated to yield substantially more

accurate MFiX-PIC results. The table below (also shown as Table 6 in the body of this report) gives the proposed calibrated settings for MFiX-PIC model parameters suggested for use in applications similar to the particle settling case. Although PSUADE-based settings have been demonstrated to give more accurate MFiX-PIC simulation results, Nodeworks-based settings were also quite good. Either group of settings may be appropriate for simulations similar to particle settling.

Validated Calibrated Model Parameters based on PSUADE and Nodeworks Results (Table 6)

MFiX-PIC Model Parameter	PSUADE Calibrated Settings for All ($\theta_1,\theta_2,\theta_3,\theta_4,\theta_5$)	Nodeworks Calibrated Settings for All ($\theta_1,\theta_2,\theta_3,\theta_4,\theta_5$)
Theta1 (θ_1): Pressure linear scale factor	14.309	18.300
Theta2 (θ_2): Vol. fraction exponential scale factor	2.165	3.590
Theta3 (θ_3): Statistical weight	12.241	7.980
Theta4 (θ_4): Vol. fraction at maximum packing	0.399	0.442
Theta5 (θ_5): Solid slip velocity factor	0.828	0.658

A separate dedicated report will demonstrate statistical calibration for the settling case. Statistical calibration will yield distributions for the model parameter settings rather than single values. Additional standalone reports will describe the calibration efforts for the fluidized bed and circulating fluidized bed applications. The overall goal of these various calibration studies is to establish validated guidance for MFiX-PIC users who are planning to carry out simulations that fall within the hypothetical flow regimes explored, and to offer a unified set of proposed calibrated settings, if possible.

1. INTRODUCTION

1.1 MOTIVATION

Particle laden flows are common in applications including chemical, pharmaceutical, energy, and food industries. Simulation-based engineering (SBE) has widely been used to optimize such systems as well as minimize their operational costs. Recently, there has been an increasing demand for modeling industrial-scale systems, where application of conventional simulation techniques like discrete element model (DEM) may be challenging. Tracking individual particles and their collisions with neighbors can become computationally intractable when particle count exceeds the order of tens of millions. Though there is rapid development in hardware resources for high performance computing, industrial scale models still may suffer from unreasonable computational turnaround times. Consequently, this issue has led to the development of particle averaging techniques such as coarse-grained DEM or particle-in-cell (PIC), which present a trade-off between solution accuracy and time to solution.

The work presented here focuses on PIC methodology developed for the open-source software MFiX (Multiphase Flow with interphase eXchanges). Even though preliminary verification and validation (V&V) studies have been completed for MFiX-PIC (Vaidheeswaran et al., 2020), evaluating the results of additional benchmark simulations, already documented for MFiX-DEM and MFiX-TFM, assists users in assessing modeling trade-offs (Musser et al., 2018; Banerjee et al., 2018).

Vaidheeswaran et al. (2021) analyzed the parametric sensitivities of different MFiX-PIC model parameters through global sensitivity analysis. Even though sensitivity analysis indicates the influence of selected parameters on quantities of interest (QoI) in a simulation, the method does not quantify ideal input parameter values. As such, the current effort explores deterministic calibration and Bayesian inference as a means to identify optimal single-value or ranged input parameters for particular MFiX-PIC simulations, respectively.

Model parameters are expected to be dependent on local hydrodynamics. In this effort, deterministic calibration of PIC parameters is performed for the case of particles settling in a dense medium, where the magnitude of fluid velocities is lower than the minimum fluidization velocity i.e., $U/U_{mf} < 1$. The input parameters and the ranges for each parameter were initially chosen based on prior sensitivity analyses.

1.2 OUTLINE

This report is the first in a series of reports designed to document input parameter calibration studies for MFiX-PIC (NETL). The report layout is arranged to help the reader first understand the PIC model parameters by considering them from a theoretical viewpoint (Section 2). Then, a background on calibration and uncertainty quantification techniques particular to this study is introduced in the context of software set-up (e.g., PSUADE and Nodeworks) (Section 3). Finally, a demonstration case is offered including calibration results (Sections 4 and 5).

The report also includes a separate data management and repository section (Appendix). There, the user is given information necessary to replicate the calibration analysis described. However, the results in this report rely on specific versions and libraries of Nodeworks, Python, and PSUADE, custom C-based code, and particular data sampling techniques (like Latin Hypercube). If the user trying to reproduce data in this work does not apply the same versions of the

employed software and pathway to solution, it should not be surprising if exact results are not replicated. However, the user should expect consistent results, provided their solution process is similarly sound.

The data management and repository section resides within NETL's Gitlab storage system, accessible at:

https://mfix.netl.doe.gov/gitlab/quality-assurance/PIC_calibration/-/tree/main/Case1_ParticleSettling/DeterministicCalibration

Note: All new users will need to register to gain access to the NETL Gitlab repository.

The purpose of the repository is two-fold: to have the information necessary to fully replicate this study, and to provide the reader with a baseline to begin their own exploration of calibration analysis. Note, however, that there is a *clear expectation* that a person accessing this repository has pre-existing knowledge of how to operate the various software associated with this study. If not, reference to the websites and user manuals of the relevant uncertainty quantification (UQ) software is advised.

2. MFiX-PIC OVERVIEW

PIC formulations are reliant on the representation of parcels, which are imagined as clumps of particles that share similar intrinsic physical properties. Specific to MFiX-PIC, each parcel is assumed to contain a group of mono-dispersed particles (so particles share both density and diameter for example). A statistical weight, W_p, indicates how many particles are in each discrete parcel. If polydisperse systems are imagined, separate solid phases are created for each particle diameter, and each phase carries a separate statistical weight. Figure 1 illustrates a polydisperse system of blue and green particles that are re-imagined as PIC parcels. Fifteen blue particles become 3 blue parcels, indicating a statistical weight of 5. Twelve green particles become 3 green parcels, indicating a statistical weight of 4.

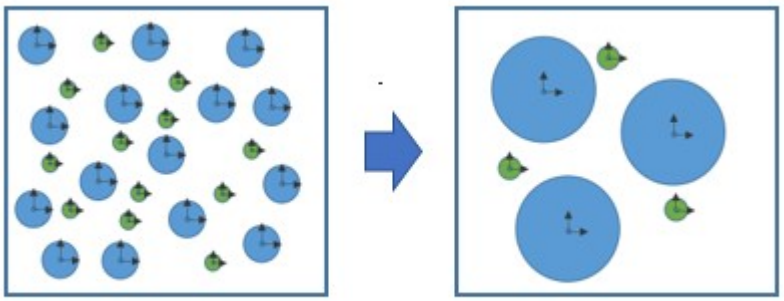

Figure 1: Visual concept of poly-disperse particle consolidation to computational parcels (Clarke and Musser, 2020). (a) A single cell populated with particles. (b) The same single cell after a statistical weight has been applied to each solid phase.

The statistical weight is used to linearly magnify expressions that are typically written at particle scale. By example, the conservation of translational momentum in the MFiX-PIC formulation is expressed as,

$$W_p m_p \frac{dU_i}{dt} = W_p(m_p g_i + \frac{m_p}{\epsilon_s \rho_s} \nabla_{\vec{x}} \tau_p) + S^{(p)}_{mi,drag} \quad (1)$$

U_i is parcel velocity in the coordinate direction i, g_i is gravitational acceleration in the coordinate direction i, ρ_s is solids density and m_p is particle mass. $_s$ is solids volume fraction and τ_p is interparticle solids stress. $S^{(p)}_{mi,drag}$ is a source term incorporating drag. Note how W_p acts as a linear operator against what would otherwise look like a traditional particle representation of translational momentum. This is typical throughout the MFiX-PIC model, where statistical weight is used to incorporate the effect of a parcel, instead of just a single particle.

Note that by default, MFiX accounts for gas-solid buoyancy through a shared gas-pressure formulation. As such, the fluid-parcel drag force acting on a parcel p is given by Equation 2 (Clarke and Musser, 2020):

$$S^{(p)}_{mi,drag} = W_p(-\frac{dP_g}{dx_i} V^{(p)} + \beta^{(p)}_g V^{(p)}(U_{gi} - U^{(p)}_i)) \quad (2)$$

where $V^{(p)}$ is the p^{th} parcel's single particle volume, $\beta^{(p)}_g$ is the p^{th} parcel's particle momentum transfer (aka drag) coefficient, and P_g and U_{gi} are the fluid phase pressure and velocity, respectively. The entire expression is then modified by the statistical weight, W_p, assigned to

parcel *p*. The drag force is added to the translational momentum equation through MFiX's general source term. A full description of particle-level calculations that are modified by statistical weight in MFiX-PIC is included in the theory document (Clarke and Musser, 2020). As an aside, the numerical implementation of the interparticle solids stress is an independent calculation within MFiX. This implies that the velocity contribution from the interparticle solids stress is incremental to the total solids velocity.

Using a statistical weight to modify grouped particle behavior is not unique to PIC methodology. By example, coarse-grain DEM follows a similar paradigm (Lu and Benyahia, 2018). Instead, the particular key to MFiX-PIC methodology is the management of an algebraic interparticle solids stress model for calculating τ_p. Newtonian mechanics is not used to derive this stress for every particle. Rather, an empirical ratio (Auzerais et al., 1988), coupled with logic (Snider, 2001) related to the sign of $\nabla\tau_p$ is employed. Specifically, the ratio used to calculate interparticle solids stress is given in Equation 3:

$$\tau_p = \frac{P_o \epsilon_s^{\beta}}{\max[\epsilon_s^* - \epsilon_s, \delta(1-\epsilon_s)]} \tag{3}$$

In this equation, the parameters P_0 and β are constants that might be conditionally specific to flow regime, where P_0 carries units of pressure. δ is any small value like ($\sim 10^{-7}$). ϵ_s is solids fraction in the cell where a parcel resides, and ϵ_s^* is a pre-determined solids fraction that represents the greatest fraction of solids that can theoretically exist in a computational cell. Note that the δ term protects against both negative and non-existent values (division by 0) of τ_p when numerical over-packing or perfect close-packing of solids may occur during calculations. Also note that τ_p is of significant value only as $\epsilon_s \rightarrow \epsilon_s^*$ and of smaller magnitude elsewhere.

It is the gradient of interparticle stress that determines whether or not τ_p will accelerate or arrest particle velocity when using the PIC method. Snider (2001) describes a simple logic to control an algebraic outcome, whereby the local PIC velocity contribution is compared to solids slip velocity. Note that solids slip velocity is the difference between individual parcel and bulk solids velocities. When the gradient of interparticle stress is less than or equal to zero, the PIC velocity contribution is positive or equal to zero. When the gradient of interparticle stress is greater than zero, the PIC velocity contribution is negative or zero. A pseudo-algorithm summarizing the above decision making has been provided as the following, but the reader is directed specifically to Equations 40 and 41 in Snider (2001).

if $\nabla\tau_p \leq 0$

PIC velocity contribution = min(δu_p,α*Slip Velocity)

PIC velocity contribution = max(PIC velocity contribution,0) else

if $\nabla\tau_p > 0$

PIC velocity contribution = max(δu_p,α*Slip Velocity)

PIC velocity contribution = min(PIC velocity contribution,0)

endif

In this logic, δu_p represents an estimated discrete particle velocity contribution from the interparticle stress calculation. What is unique to MFiX-PIC with regard to the above logic sequence is that a user-controlled factor, α, can be applied to the solids slip velocity to dampen or enhance its effect in the described comparisons.

As MFiX-PIC has gone through performance evaluation, effort has been made to evaluate how the various user-controlled parameters affect solutions. The most obvious PIC parameters are the values that populate the interparticle stress equation, specifically, $P_0, \beta,$ and ϵ_g^*. Published works indicate that tuning the linear pressure factor (Andrews and Snider, 1995; Snider, 2001, 2007; Snider et al., 2011) and exponential scale factor (Auzerais et al., 1988; Snider, 2001) is necessary to capture specific flow regime types. In general terms, P_0 is set to less than 10 Pa in simulations that do not experience dynamic flow (like settling) and greater than 100 Pa in simulations with considerable particle motion (like circulation). These *rule of thumb* observations are described through a tentative flow regime map in Figure 2, whose axes are pressure linear scale factor P_0 and normalized velocity of the continuous phase $\frac{U}{U_{mf}}$. However, the goal of this study is to provide better and more specific ranges, not only for P_0, but for all keyword accessible MFiX-PIC parameters considered including β, the solids volume fraction exponential scale factor and ϵ_g^*, close packed volume fraction. Before this study, advice was simply to set $2 < \beta < 5$, and the encouragement to choose close packed volume fraction in a way consistent with physical expectations based on particle size distribution and polydispersity (Dexter and Tanner, 1972; Thies-Weesie and Philipse, 1994; Desmond and Weeks, 2014).

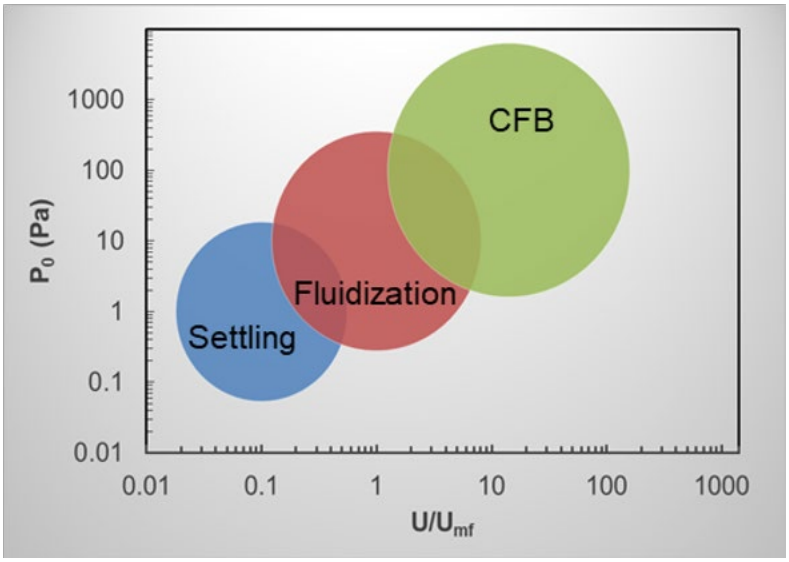

Figure 2: Hypothetical flow regime map (Vaidheeswaran et al., 2020).

Proper selection of W_p, statistical weight of particles, or more easily, number of particles per parcel is not well defined in literature. On one hand, users want to limit the number of parcels in a system to reduce the overhead of tracking individual entities. On the other hand, users want to maintain as many parcels as possible to best reflect a system that is really made up of many more

particles to best capture physical dynamics. These considerations must be balanced with the proper reflection of solids fraction per cell in a simulation (for as statistical weight increases, the ability to tune solids fraction deteriorates). Consequently, estimates have evolved within the MFiX-developers community where 20 parcels/computational cell at close-packed conditions is considered some kind of lower threshold for particle representation.

Finally, there is the effect of α, a linear coefficient that modifies solid slip velocity. Again, there is no body of literature to help a user select this value. MFiX-developers realized that when α=1, numerical overpacking often occurred in settling simulations, but when α=0.5 that overpacking abated. Such numerical sensitivity was not observed in simulations that involved very active particle motion, but MFiX developers have yet to create a suggested range of values convenient to users.

As MFiX-PIC development continues, creating PIC parameter ranges for the general user community has become more important. This study demonstrates the preliminary steps by purposefully defining ideal values for the above parameters in the context of diverse simulation cases: particle settling, a fluidized bed, and a circulating fluidized bed. In addition, this study assesses the sensitivity of the aforementioned parameters so that a user can knowledgeably employ the insight gained to tune their application simulations.

3. METHODOLOGY AND SOFTWARE FRAMEWORKS EMPLOYED

Several advanced UQ methods and UQ software toolkits were used in the MFiX-PIC calibration analysis presented in this report. As such, this section provides a brief overview of these methods and toolkits. Note that the intent of this report does not include the theoretical underpinnings of statistical analysis as it relates to calibration, nor how to use associate software; therefore, in each subdivision of this section, additional references are provided to direct the user to more comprehensive guidance if required.

3.1 SIMULATION CAMPAIGNS AND SURROGATE MODEL CONSTRUCTION

Calibrating input parameters for computational simulation first requires a user to define *QoI/response variables*. These are measurable values that can universally help in assessing the accuracy of a simulation. There may be many input parameters that affect these quantities of interest, and the effect of changing those parameters may be interrelated. For example, to calibrate 5 input parameters for a single response variable might require thousands of evaluations to find an optimal set of parameters that yield the smallest residual between a simulated and experimental QoI. To avoid running these thousands of simulations, it is common to construct a surrogate model (a.k.a. a response surface or meta-model) and use it to predict simulation outcomes instead.

Surrogate models are numerous and vary in form and function. In this study, a data-fitted surrogate model, which characterizes the relationship between a response variable and input parameters through sampling simulations that span user prescribed ranges of input parameters was created. In this work, the language *simulation campaign* describes carefully designed samples of simulations, chosen to create a numerical relationship between input parameters and a response variable. In this approach, the simulation code (i.e., MFiX-PIC) is treated as a black box and executed for each sampling simulation as part of a larger predetermined simulation campaign.

Intuitively it seems the number of sampling simulations in a simulation campaign must play a critical role in constructing a reliable data-fitted surrogate model. In fact, simulation campaigns are designed using a mathematically defined space-filling property to assure enough sampling points within the range of each input parameter are represented. One common sampling method for computational experiments is Latin Hypercube (LH) sampling (Viana, 2013). In this study, a particular Optimal Latin Hypercube (OLH) sampling method is employed whereby a distance metric effectively distributes input parameters to fully span user-defined ranges while ensuring samples are located far from each other.

The workflow outlined below was followed to design the simulation campaign and to construct the data-fitted surrogate models:

1. Identify the model input parameters to be varied systematically as part of the sampling simulations, and the QoI to be extracted from the results. To bring all stakeholders together and to minimize future disagreements, a survey (Gel et al., 2018) was employed to capture detailed information from the researchers, subject matter experts, and other stakeholders involved. After several iterations, the survey provided a clear picture of critical issues like how many input parameters would be explored and what the lower and upper bounds of these parameters would be within the simulation campaign.

2. Design the simulation campaign employing OLH sampling principles. In this case, 6 model input parameters were identified within certain ranges. Although the simulation campaign was carried out for 3 quantities of interest, for deterministic calibration only the second QoI (i.e., location of filling shock) was considered. Using 20 samples per input parameter, an initial simulation campaign of 120 samples was designed.
3. Launch and monitor the simulation campaign, preferably on a HPC system.
4. Post-process the results from simulations to construct a tabular dataset where each row shows the 6 model parameter settings and simulation results for each of the QoI corresponding to that sampling simulation.
5. Post-process the converged simulation campaign results and compile an ASCII file for the tabulated dataset. This file consisted of the design of experiments for the model parameters and the corresponding quantities of interests from the simulation campaign results.
6. Import the tabulated dataset into UQ toolkit software employed, and test different surrogate model options to determine the best data-fitted surrogate model for the given dataset using various statistical metrics. For example, cross-validation error assessment was employed to assess the quality of the data-fitted surrogate model.

Once a best data-fitted surrogate model was identified, this same surrogate model was used throughout the subsequent calibration process in lieu of further MFiX-PIC simulations. The construction of the data-fitted surrogate model was the most time-costly part of this calibration effort. For a detailed discussion related to surrogate model construction, including error minimization, the reader is referred to earlier studies (Gel et al., 2013a,b; Gel et al., 2016).

3.2 SENSITIVITY ANALYSIS

Sensitivity analysis is one uncertainty quantification technique employed to address the important question: “Which input parameters have the most influence on a quantity of interest?” For calibration purposes, sensitivity analysis plays a key role, particularly when the number of input parameters exceeds 3. The technique quantitatively determines the most influential parameters for each quantity of interest, and can be used to focus the attention of experimentalists, particularly when resources are limited. In the current study, sensitivity analysis identified 2 key input parameters. Had experimental resources been slim, this would have immediately refocused the calibration effort and minimized physical testing. However, the problem of interest in this study (particle settling) has an analytic solution, so no physical experimentation was necessary, and the full sweep of input parameters identified by stakeholders was investigated. However, for follow-up cases (fluidized bed and circulating fluidized bed), the experimental dataset will be limited, and sensitivity analysis is expected to play an important role in guiding the calibration efforts. Hence, the methodology is introduced here.

The sensitivity analysis results shown later in this report (Figure 11) were obtained using the Sobol’ indices based global sensitivity method, which is the preferred methodology for cases with non-linear response behavior. The data-fitted surrogate model was used to perform function evaluations for computing the QoI when calculating the Sobol’ indices. The reader is referred to Sobol (2001) and Iooss and Lemaître (2015) for additional information on the methodology, and Gel et al. (2013a,b) for a demonstration with multiphase flow simulations. Additionally, a

detailed sensitivity analysis study performed for the problem of interest with Nodeworks software can be found in (Vaidheeswaran et al., 2021).

3.3 CALIBRATION

Computational models often incorporate empirical input parameters as well as physically observable input parameters. By example, in MFiX-PIC, only close packed volume fraction would be considered physically observable; all other input parameters are empirical. The intent of calibration is to tune input parameters with the aid of observable data (e.g., experiments) so that a computational model reproduces expected physics in simulations.

Figure 3 shows a simple sketch to illustrate the objective of calibration (Adams et al., 2015). For this example, assume the transient temperature behavior in a fluidized bed reactor is being analyzed. Let the temperature profile in time be represented as the blue line. This is the target of simulation, most likely observations from sensors or measurements from experiments. Then consider a computational model, $s(t;\theta)$, that aims to capture the temperature behavior in time (red line) through simulation. The model requires various input parameters, θ, to execute (e.g., heat transfer coefficient). Recall that most computational models represent a simplification of actual governing physics by employing assumptions, so they will not capture exact physical behavior, hence there is discrepancy between the targeted and simulation results, as illustrated.

Although some model input parameters might have theoretical foundation, the settings employed for these parameters during simulations are usually considered uncertain. The calibration process aims to minimize the difference between the target and simulation output by adjusting the settings for the θ parameters. This is accomplished with the guidance of observations or experimental data representing the target. By reducing the disparity between targeted and simulation results, calibration plays an important role in increasing the credibility of a simulation for a particular application.

At this point it is important to note the difference between validation and calibration. Validation is direct comparison of simulation results to experimental results without tuning. One might use validation to establish a baseline discrepancy between an experiment and a simulation, and use that information to justify the need for model calibration. Both validation and calibration are always performed against a specific set of observable data, which makes the credibility of the experimental data quite critical. Careful consideration must be given when generalizing the insights gained as a result of calibration studies, particularly when applying previously calibrated input parameters to new simulations. The reader is referred to Trucano et al. (2006) for further information on the difference between validation and calibration.

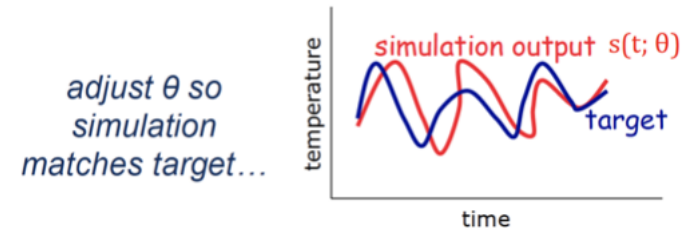

Figure 3: Illustration of computational model calibration from DAKOTA training on calibration (Adams et al., 2015).

Typically, there are multiple input parameters (i.e., $\theta_i, i = 1,n$) that need to be calibrated concurrently. This situation poses unique challenges especially if experimental data is limited. Consequently, many different calibration approaches are found in literature (Adams et al., 2015).

In general, calibration methods are categorized under two groups: (i) deterministic calibration methods, and (ii) statistical calibration methods. The latter provides a distribution for the calibrated model parameters instead of single values, which is the outcome of deterministic calibration. Another major difference is the ability of statistical calibration to take into account model bias (a.k.a. model form uncertainty) while performing calibration of model input parameters. However, statistical calibration methods usually require the knowledge of complex methods and algorithms such as Markov Chain Monte Carlo (MCMC). Deterministic calibration is easier to understand and widely implemented in various software tools that have optimization capability.

3.4 DETERMINISTIC CALIBRATION

The goal of deterministic calibration is to find values of $\boldsymbol{\theta} = \{\theta_1 \dots \theta_m\}$ that will minimize residual error between a group of simulations and their equivalent experimental counterparts. Equation 4 acts as the objective function for the optimization problem (Adams et al., 2015). It represents the sum of squares of the residual errors introduced by employing this set of $\boldsymbol{\theta}$ in n simulations.

$$\underset{\boldsymbol{\theta} \in R}{\text{minimize}} f(\boldsymbol{\theta}) = \sum_{i=1}^{n} [S_i(\boldsymbol{\theta}) - y_i]^2 = \sum_{i=1}^{n} [R_i(\boldsymbol{\theta})]^2 \tag{4}$$

where $\boldsymbol{\theta} = \{\theta_1 \dots \theta_m\}$ are the modeling parameters being calibrated
y_i is the i^{th} experiment data observed out of n experiments
$S_i(\boldsymbol{\theta})$ is the simulation result for i^{th} experiment data as function of $\theta_1 \dots \theta_m$
$R_i(\boldsymbol{\theta})$ is the i^{th} residual (simulation - experiment)

Depending on the nature of the problem there are various local and global optimization techniques that could be employed to solve the residual minimization problem shown in Equation 4. In this light, an important distinction between statistical calibration and deterministic calibration is that the outcome from statistical calibration is an estimated distribution of the $\boldsymbol{\theta}$ parameters individually, whereas deterministic calibration provides a single scalar value for each of the model parameters being calibrated.

Workflow for Deterministic Calibration

The workflow outlined below was followed to perform deterministic calibration in this study. For a visual perspective, the same workflow is illustrated in Figure 4:

1. Identify the model parameters to be calibrated, and determine the lower and upper bounds for each of these parameters to be used during calibration.
2. Prepare an experimental dataset or observations to be used to guide the calibration process as an ASCII input file.
3. Plan a simulation campaign with the aid of statistical design of experiments principles that will enable the construction of a data-fitted surrogate model. The surrogate model should adequately characterize the relationship between model parameters considered as input and the response variables (a.k.a. QoI or output). This step is crucial when the

simulations are expensive or time consuming to perform as the optimization process requires thousands of function evaluations to be performed cheaply.

4. Post-process the simulation campaign results and compile an ASCII file as a tabulated dataset consisting of the design of experiments for the model parameters and the corresponding QoI from the simulation campaign results. For calibration, a separate dataset containing the experimental observations is necessary. This should be prepared in ASCII format for importing into UQ software. For the current application, an analytical solution was available and used in lieu of experimental observation data. Twenty-one samples were created by varying the control parameter (x_1: Initial solid concentration).
5. Utilize UQ toolkit (PSUADE, Nodeworks) to import the datasets and perform the optimization required to minimize the residuals in Equation 4. The minimization procedure may necessitate multiple attempts, which will generate several sets of values for θ_i, $i = 1,n$. Each attempt will yield a minimum residual for all experimental samples. A parallel coordinates plot that incorporates all of the proposed settings of θ_i, $i = 1,n$ is utilized to identify the most frequently encountered values. Note that the surrogate model constructed is used to perform the evaluations required for $S_i(\boldsymbol{\theta})$ in Equation 4 in lieu of actual MFiX-PIC simulations for each instance. Hence, the credibility of the surrogate model needs to be carefully assessed prior to the optimization step with measures such as adjusted R^2 or cross-validation error assessment. Doing so ensures the error introduced by the surrogate is minimized.
6. Verify the proposed calibrated model parameter settings by re-running a select group of simulations within the existing simulation campaign or by constructing a new simulation campaign for unseen samples. In both cases, any error needs to be assessed against an experimental solution to determine whether the calibrated settings truly improve the credibility of the simulation model for the targeted application.

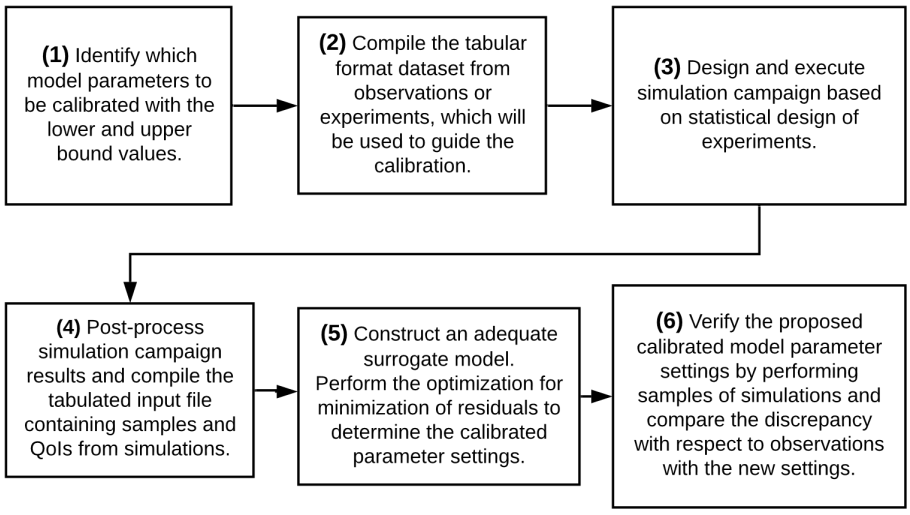

Figure 4: Illustration of the deterministic calibration workflow performed in this study.

For the scope of the current study only deterministic calibration analysis was performed. A follow-up study and technical report will demonstrate the results of the statistical calibration for the same problem and compare the outcomes from both approaches.

3.5 SOFTWARE TOOLBOXES EMPLOYED

Two open-source UQ software were employed in this study: PSUADE (Tong, 2010, 2020) and Nodeworks (NETL, 2020; Weber et al., 2020). The primary differences between the two software are available surrogate model options and optimization algorithms. Because this is a first-of-kind calibration study for MFiX-PIC, a secondary objective whereby the proposed calibrated model settings from each software tool were compared to each other was incorporated into the overall research effort. Below, a brief overview of each software is offered.

PSUADE

PSUADE is an open-source UQ software toolkit developed at the Lawrence Livermore National Laboratory by Dr. Charles Tong (Tong, 2010) and released under Lesser General Public License (LGPL) license since 2007. The name of the software, PSUADE, comes from the acronym for Problem Solving Environment for Uncertainty Analysis and Design Exploration. The program supports a variety of non-intrusive uncertainty quantification analysis methods where the simulation application can be treated as "black-box" code. Subsequently, many UQ analysis tasks can be performed by sampling the black-box directly or through a data-fitted surrogate model constructed from the computational model. The software offers a diverse range of sampling methods to enable users to perform simulation campaigns with the objective of constructing an adequate data-fitted surrogate model (a.k.a. response surface model, meta-model). The user can perform both basic uncertainty analysis such as forward propagation of uncertainties and more complex analysis like mixed aleatory-epistemic uncertainty analysis. PSUADE has a built-in statistical calibration capability (i.e., Bayesian calibration with MCMC). However, deterministic calibration required user-defined supporting code to incorporate residual evaluations. PSUADE is written in C++ and operates primarily as a command line-based software, which may require some learning curve. Additional details on the capabilities of PSUADE can be found at the website of the software (Tong, 2020).

Nodeworks

Nodeworks, developed at the NETL, is an open-source graphical programming interface library and workflow framework where users can add, delete, and connect nodes to create customized visual workflows (NETL, 2020; Weber et al., 2020). Nodes perform prescribed operations on data whose results are then passed to other nodes using connections. The library was specifically developed in the Python programming language to remain flexible and portable. It can support a wide variety of applications and contains several collections of default nodes to assist deployment of commonly used workflows quickly, even for novice users. Users can also create and add custom nodes for specific applications. This work leverages a collection of nodes known as the *Surrogate Modeling and Analysis Toolset,* which was developed to implement workflows that construct and use data-fitted surrogate models/response surfaces. The Surrogate Modeling and Analysis Toolset provides access to specialized nodes including optimization, sensitivity analysis, forward propagation of uncertainty, and Bayesian calibration.

Additionally, Nodeworks is directly embedded into MFiX's graphical user interface (GUI), thus allowing Nodeworks to create input decks with parametrically varying inputs directly. This allows for simple set-up and management of simulation campaigns. Similarly, Nodeworks can be employed by other modeling software to create workflows with ease.

4. CALIBRATION DEMONSTRATION CASES

4.1 OVERVIEW OF DEMONSTRATION CASES CONSIDERED

MFiX-PIC is an attractive software for examining industrially relevant applications. This report documents the beginning of a course of calibration studies that will examine 3 industrial applications that span a wide range of flow regimes. In particular, the studies/cases are particle settling, a fluidized bed, and a circulating fluidized bed. Note that this first report concentrates on the particle settling problem, in the context of deterministic calibration.

The objective of a deterministic calibration study is to obtain a set of optimal model parameters for a given application problem. Ultimately, the authors of this report hope to provide the MFiX-PIC user community with a set of default settings for input parameters that will serve as good starting points in their own examination of similar industrial problems.

4.2 GRAVITATIONAL PARTICLE SETTLING

The problem of visualizing particles settling under gravity in a dense medium has an analytical solution. This means that a well-controlled experiment would give exactly the same result as a hand-calculation. From a calibration standpoint, this implies that there is no worry of added experimental error when evaluating any hypothetical physical set-up. Any hand-calculation for the solution is *the truth*. This indicates that the question of error moves entirely to the surrogate model that is created by the simulations in the simulation campaign.

The setup, borrowed from Vaidheeswaran et al. (2020), is described in Figure 5. The computational domain considered is 0.02 m (x-direction) × 0.02 m (z-direction) × 1 m (y-direction). Uniform grid sizes of 4 mm are used in the x- and z- directions, while a grid size of 2 mm is used in the y-direction. Each simulation uses a constant time-step size of 5e-4 s and is run for a total duration of 1 s.

Once the simulation begins, two concentration (kinematic) shocks evolve. The first originates from the top of the particle bed and corresponds to settling, while the other originates from the bottom of the imagined vessel and corresponds to a filling shock. The location of the filling shock (y_2) is the QoI considered in this study. Its analytical solution is given by:

$$y_2(t) = -t\left(\frac{\epsilon_s^*\epsilon_g^* u_r^* - \epsilon_{s0}\epsilon_{g0}u_{r0}}{\epsilon_s^* - \epsilon_{s0}}\right) \tag{5}$$

where ϵ_s^* and ϵ_g^* are volume fraction of solids phase and gas phase at close-packing conditions.

ϵ_{s0} and ϵ_{g0} are initial volume fractions. u_r^* and u_{r0} represent relative velocities calculated using close-packing and initial conditions, respectively. The filling shock propagates upward when a lower region is fully packed by solids. Properly predicting the filling shock may correspond well to other simulations where solids concentration is high and particle motion is relatively slow.

The location of the settling shock (y_1) is another QoI post-processed from the simulations. This shock propagates in the direction of gravity, and corresponds to the transition between homogeneously distributed solids with concentration ϵ_{s0} and a dilute region where $\epsilon_s = 0$. The analytical solution for y_1 is given by Equation 6,

$$y_1(t) = x_0 - t\,(\epsilon_{g0} u_{r0}) \tag{6}$$

Average void fraction at the first cell location (y_3) is the final QoI post-processed from simulations. However, both y_1 and y_3 are not considered in the current deterministic calibration study. In the remainder of the report, the only QoI considered is the location of the filling shock (y_2). Using Equation 5, a standalone dataset was generated at 21 different x_1 settings where x_1 is equivalent to ϵ_{s0}, the initial solids concentration. Note that it is this dataset, consisting of 21 samples, that is used in lieu of experimental data required for deterministic calibration.

Previously, Vaidheeswaran et al. (2020) used this settling case to compare default setting results from MFiX-PIC, MFiX-TFM and MFiX-DEM simulations as shown in Figure 6. Plots show time evolution of concentration fronts from the 3 models with the analytical solution when ϵ_{s0} = 0.15.

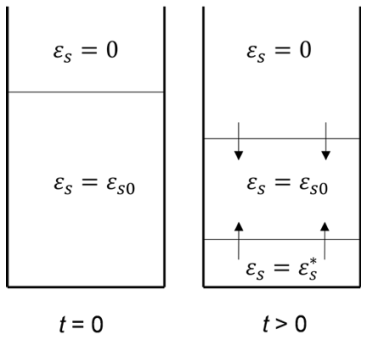

Figure 5: Schematic of particles settling in a dense medium.

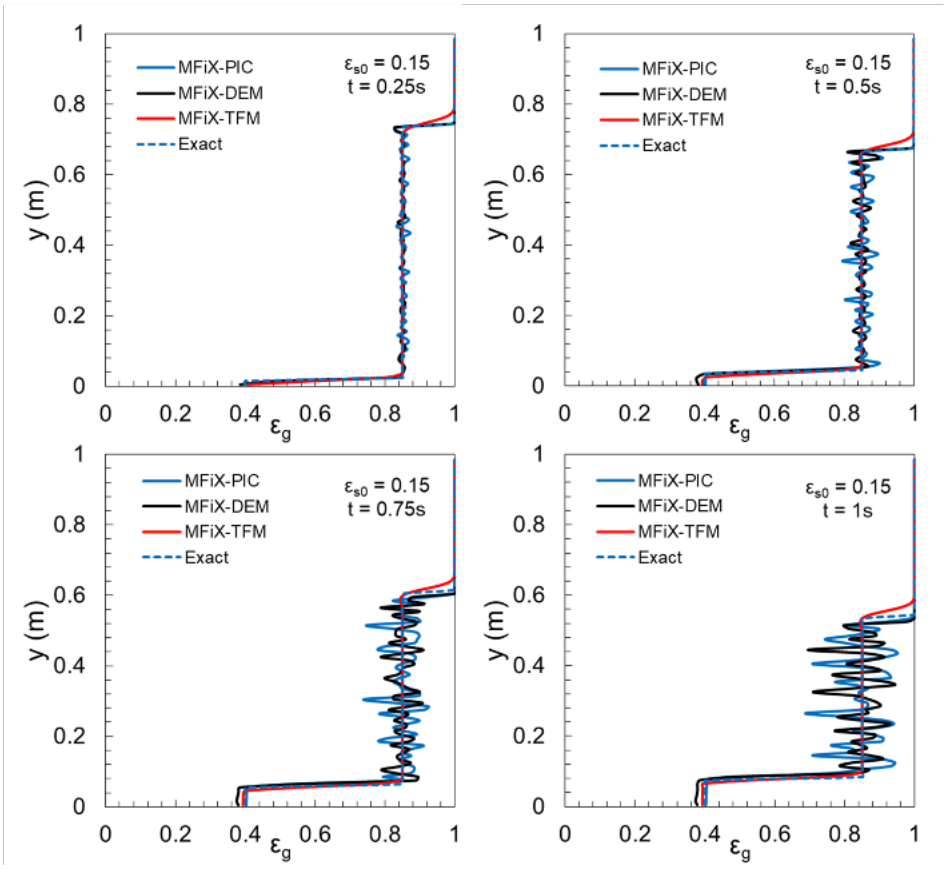

Figure 6: Comparison of time evolution of shock fronts obtained using uncalibrated MFiX-DEM, MFiX-PIC, and MFiX-TFM simulations with the analytical solution.

Simulation Campaigns

Prior to any calibration work, a simulation campaign was carefully designed and executed to create an adequate surrogate model. This surrogate model was then used in lieu of actual MFiX-PIC simulations to provide cheaper evaluations of the QoI needed during the calibration study.

Design of Sampling Simulations: An OLH sampling method was used to generate a sampling campaign for 6 MFiX input parameters. The first 5 were modeling parameters specific to MFiX-PIC, accessible to the user through keywords. These included: θ_1 : Pressure linear scale factor (P_0); θ_2 : Volume fraction exponential scale factor (β); θ_3 :Statistical Weight (W_p); θ_4 : Void fraction at maximal close packing (ϵ_g^*); and θ_5 : Solids slip velocity scale factor (α). The sixth parameter was initial solids concentration, a general input parameter used to specify an initial condition in MFiX, regardless of model. In the remainder of this report, abbreviated versions of the input parameter names might have been used due to font issues in plotting software. Table 1 offers these abbreviations along with lower and upper bound values used for each model parameter in the simulation campaign. For example, anywhere t1:P_0 or t1 or Theta1 appears in this report, it is equivalent to θ_1:Pressure linear scale factor (P_0).

Table 1: List of Input Parameter Abbreviations, Descriptions, Lower and Upper Bounds Values Considered in Simulation Campaign

Symbol	Description	Min.	Max.
θ_1 or t1:P_0	Pressure linear scale factor, (P_0)	1.0	20.0
θ_2 or t2:beta	Volume fraction exponential scale factor, (β)	2.0	5.0
θ_3 or t3:StatWeight	Statistical Weight, (W_p)	3.0	20.0
θ_4 or t4:ep_g*	Void fraction at maximal close packing, (ϵ_s^*)	0.35	0.5
θ_5 or t5:VelfacCoeff	Solids slip velocity scale factor, (α)	0.5	1.0
x_1	Initial solids concentration, (ϵ_{s0})	0.05	0.25

The initial QoI (a.k.a. response variables) extracted from the simulation campaign were, y_1:Location of Settling Shock; y_2:Location of Filling Shock; and y_3:Void fraction in the first cell nearest to the bottom of the experimental vessel. The scope of the work presented herein is to analyze the performance of MFiX-PIC in regions having dense concentration of particles. Because of this, only y_2 is used in this analysis. This analysis is assessing PIC parameters in regions having intermediate to dense solids concentration, and hence does not consider y_1 , which marks the transition between initial solids concentration ϵ_{s0} and $\epsilon_s = 0$. y_3 is discounted because it would be compared against single values, and hence not compatible with the calibration framework. Although all three QoI were party to analysis in the simulation campaign, only y_2:Location of Filling Shock was considered the key QoI for calibration purposes. Note that in the remainder of this report, abbreviated versions of this QoI name might have been used due to font issues in plotting software such as y2:LocFilling corresponding to y_2 :Location of Filling Front or Shock.

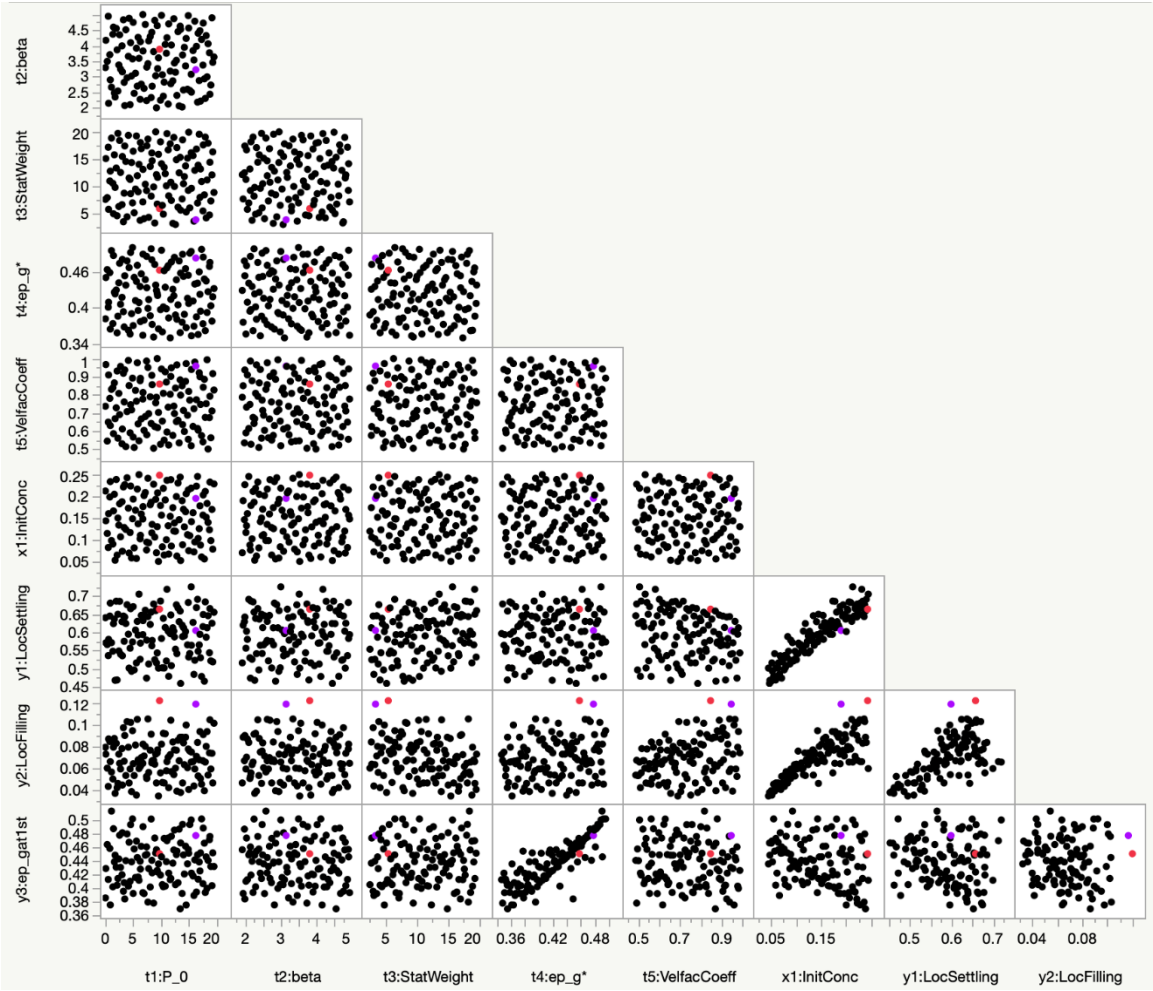

Figure 7: Scatter matrix plot of all input parameters and QoI employed in the simulation campaign using OLH design base (120 samples) with potential outlier samples for y_2:LocSettling highlighted in red and purple colors.

Figure 7 shows a scatter matrix plot of all input parameters and QoI. This type of image can be used to make a quick visual assessment of obvious correlations. For example, Figure 7 indicates that there is a strong linear correlation between Initial Concentration ($x1$, on horizontal-axis) and Location of Settling Shock ($y1$, on vertical-axis); this evaluation is based on examining the block representing ($x1$ v. $y1$) as an independent graph and noting a generally linear correspondence between the variables. Likewise, similar somewhat linear correspondences can be seen in the blocks ($t4$ v. $y3$) and ($x1$ v. $y2$).

This type of qualitative visualization is also useful in identifying any apparent outliers among the QoI such as samples # 42 and # 51, which are highlighted in red and purple colored circles, respectively. The identification of outliers can be done visually, as these data points will appear apart from the majority of other data points. By example, focusing on the row of plots associated with $y2$, samples #42 and #51 consistently appear separate from other data points. Another way to identify outliers is by using the kernel density estimation, a quantitative non-parametric

method to estimate probabilities for new points. Although not shown in Figure 7, when kernel density estimates are computed and plotted, samples # 42 and # 51 appear where a kernel density estimate is relatively low. Hence, these two samples are most likely outliers.

Outliers can be caused by non-converged simulations or unique input settings that create an extreme result for the QoI. Assessment of simulation outcomes is uniquely important at this stage as only physically sound results should be used to construct the data-fitted surrogate model. Note that among the 120 samples shown in Figure 7 there were not any other apparent outliers for the QoI, $y2$.

Figure 8 shows a parallel coordinates plot, a means of visually translating a tabular dataset into a coordinate map. Each input parameter is presented along the horizontal axis, then ranged upward along a single line regardless of unit. For example, Figure 8 represents a dataset that has been constructed from a table with header labels $[t1|t2|t3|t4|t5|x1|y2]$; $t1$ varies between 0 and 22.5; $t2$ varies between 2 and 5, and so on. If unfamiliar with the technique, the reader is referred to (Heinrich and Weiskopf, 2013) for additional information about parallel coordinates plot-based visualization.

In the context of this work, the parallel coordinates plot shows when the QoI, $y2$, clusters unexpectedly or seems to become an outlier. For example, red and purple lines identify outliers of $y2$ in Figure 8, which were also identified as samples #42 and #51 in Figure 7. By following these lines back through the input parameters, one can ask, *Is there something unusual about these parameter settings?* and use this information to guide decision-making as it relates to the construction of the surrogate model such as deciding to perform additional simulations to improve the likelihood of constructing an adequate surrogate model.

A preliminary investigation was carried out by filtering the $t3$ and $t4$ settings based on the information obtained from the two outliers. Figure 9 shows the revised version of the parallel coordinates plot where an investigation was performed to see if the samples identified as outliers have anything to do with particular ranges of values for $t3$ or $t4$. Specifically, all samples with $t3 \leq 5.8904$ and $t4 \geq 0.4621$ are shown. The values were determined based on the corresponding $t3$ and $t4$ settings for samples #42 and #51.

Insight gained from Figure 9 may not be adequate to conclude that a combination of lower end values of $t3$ or higher end values of $t4$ are correlated with the observed outlier behavior. For example, adding higher end values of $t5$:VelfacCoeff to the previous settings might yield a different conclusion. Parallel coordinates plots simply provide different ways to visualize and derive insights from the simulation campaign dataset.

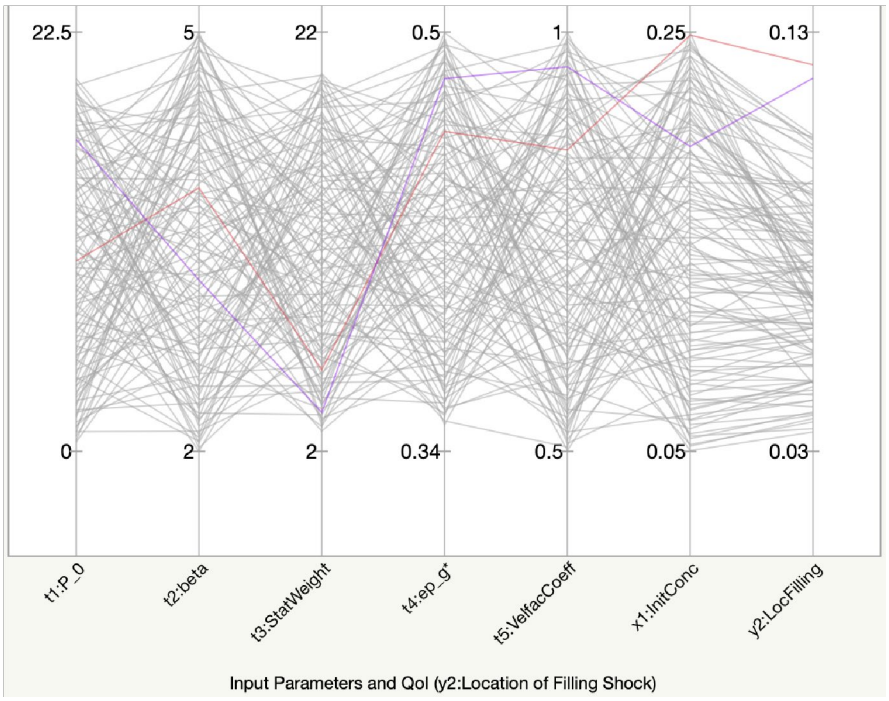

Figure 8: Parallel coordinates plot of all input parameters and second QoI ($y2$: Location of Filling Shock) in simulation campaign using OLH design base (120 samples).

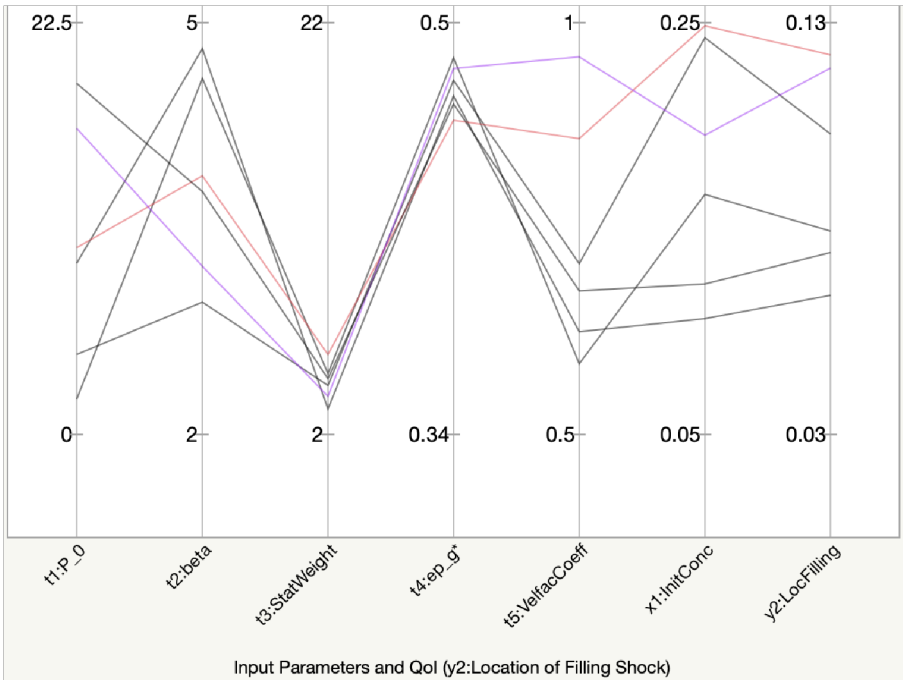

Figure 9: Revised parallel coordinates plot of all input parameters and second QoI ($y2$: Location of Filling Shock) by showing only samples with $t3 \leq 5.8904$ and $t4 \geq 0.4621$.

Surrogate Model Construction:

After post-processing, results of the sampling simulations were used to construct a data-fitted surrogate model. Recall that the surrogate model is intended to replace MFiX-PIC simulations during UQ analysis. Construction is critical particularly when simulation is expensive and/or time consuming.

Several surrogate model types were explored during the construction process. These included MARS, linear regression, and the Gaussian process model. In the end, a Gaussian process model (Tong implementation in PSUADE under option 10) appeared to provide one of the best fits based on the root mean square error (RMSE), which was calculated by PSUADE to be 6.61e-03 for the data-fitted surrogate model. The input file for the PSUADE data fitted surrogate model is provided in Appendix A.

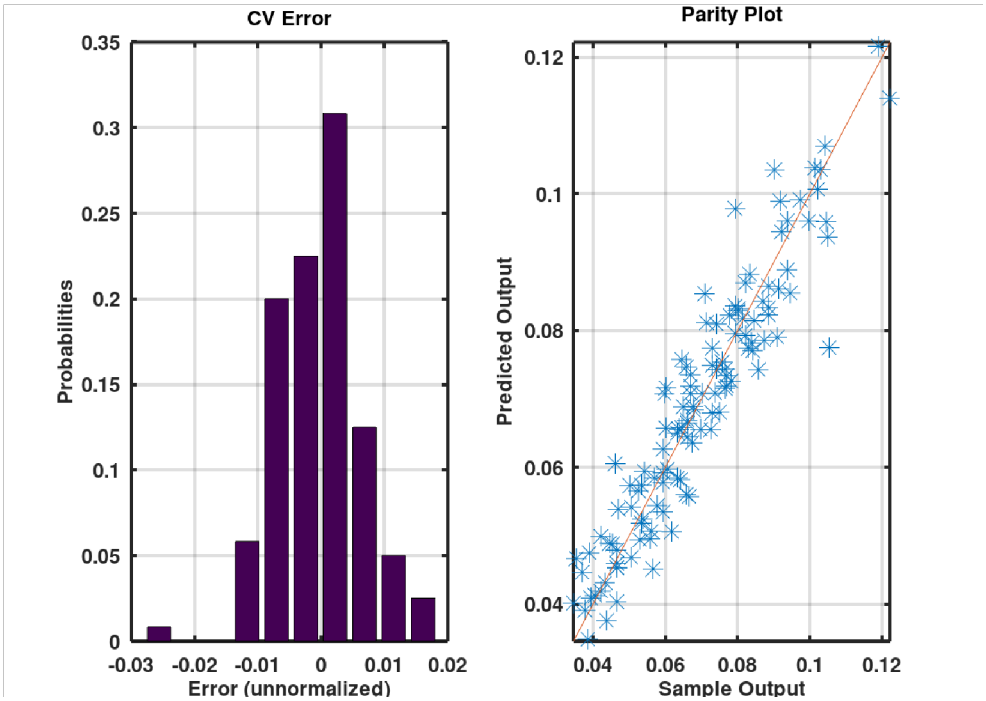

Figure 10: Assessment of the quality of the surrogate model through cross-validation errors.

Figure 10 shows cross-validation error assessment results created with PSUADE. The parity plot on the right compares actual MFiX-PIC simulation results (horizontal axis with "Sample Output" label) with the surrogate model's predictions (vertical axis with "Predicted Output" label). Ideally, sample points should fall along a 45° line through the parity plot shown in red color. Any deviation from the 45° red line reveals discrepancy between the simulation and data-fitted surrogate model, which implies an additional level of uncertainty being introduced when the surrogate model is used in lieu of the corresponding MFiX-PIC simulations. To better illustrate the error between simulation and data-fitted surrogate model, the histogram on the left reveals how the deviation from the diagonal is distributed. Ideal distribution of errors is expected to be

centered around zero and have tails without any skew. The histogram shows some skew most likely due to the outliers observed.

Global Sensitivity Analysis:

Prior to the deterministic calibration study, a global sensitivity analysis was performed using Sobol' indices in the PSUADE UQ Toolkit. Although a previous sensitivity study was carried out in Nodeworks (Vaidheeswaran et al., 2021), this separate global sensitivity study was performed to incorporate an additional input parameter (x_1:Initial concentration). The additional parameter reflects the analytical solution's natural dependency on x_1.

Figure 11 shows the Sobol' total sensitivity analysis results, which assess the most influential parameters on the QoI, y_2:Location of Filling Shock. It is important to note that Total Indices take into account both main effects and their interaction effects on the QoI. For the 120 sample simulation campaign results, x_1:Initial Concentration appears to have the most pronounced effect on y_2. The green symbols show the confidence interval associated with 100 sample bootstrapping for each parameter. Confidence intervals do not show significant variability for any Sobol' index estimated.

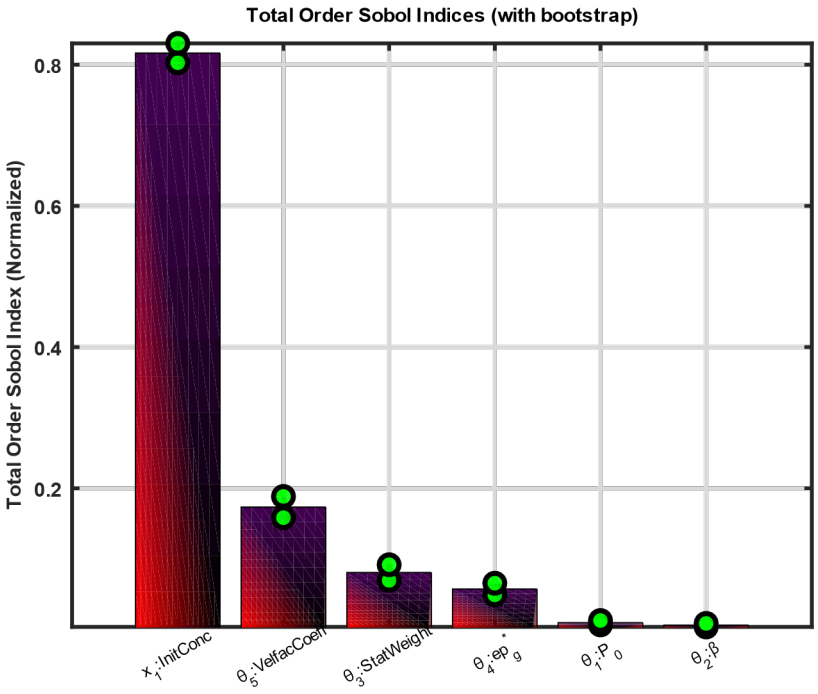

Figure 11: Global sensitivity analysis results based on the 120 sample simulation campaign dataset.

Deterministic Calibration with PSUADE UQ Toolkit:

Table 2 shows one of the proposed settings for the five modeling parameters obtained at the end of the deterministic calibration procedure. Recall that this process involved deterministic

optimization, which finds the values of $\boldsymbol{\theta} : \{\theta_1 \ldots \theta_5\}$ that minimize the residuals shown in Equation 7.

$$\underset{\boldsymbol{\theta},\mathbf{x}\in R}{\text{minimize}} f(\boldsymbol{\theta},\mathbf{x}) = \sum_{i=1}^{n}[S_i(\boldsymbol{\theta},\mathbf{x}) - y_i(\mathbf{x})]^2 = \sum_{i=1}^{n}[r_i(\boldsymbol{\theta},\mathbf{x})]^2 \quad (7)$$

where $\boldsymbol{\theta} = \{\theta_1, \theta_2, \theta_3, \theta_4, \theta_5\}$ are the modeling parameters being calibrated
$\mathbf{x} = \{x_1\}$ is the physical control parameter (initial solids concentration)
$y_i(\mathbf{x})$ is the i^{th} experiment data observed out of n experiments
n is total number of experimental data, which is 21 for the current case
$S_i(\boldsymbol{\theta},\mathbf{x})$ is the simulation result for i^{th} experiment data
as function of $\theta_1 \ldots \theta_5$ and x_1
$r_i(\boldsymbol{\theta},\mathbf{x})$ is the i^{th} residual (simulation - experiment)

There are various optimization techniques that may be employed to solve the residual minimization problem. In this case, the constructed data-fitted surrogate model is used to evaluate the $S_i(\boldsymbol{\theta},\mathbf{x})$term instead of running MFiX-PIC simulations.

The deterministic calibration results presented in Table 2 were obtained with PSUADE UQ software (Tong, 2010) through the following steps:

1. Post-process and import the simulation campaign results into a format that PSUADE can read, i.e., standard ASCII text file with tabulated data where each column represents the input parameters considered and the quantity of interest. For this case, 6 columns of input ($\theta_1 \ldots \theta_5$, and x_1) and 1 column of QoI ($y2$: Location of Filling Shock) were employed. For formatting purposes, the first row of the file indicates total number of samples, total number of input parameters, and total number of quantities of interest.
2. Construct a data-fitted surrogate model in PSUADE to characterize the relationship between input parameters and QoI, which in turn will be used for quick and cheap function evaluations needed during the optimization process. To minimize the effect of surrogate model related uncertainties, test the adequacy of the constructed surrogate model by employing cross-validation error assessment and other statistical measures such as R^2 if employing a polynomial regression based surrogate model. The goal is to find the best suited data-fitted surrogate model for the given dataset.
3. Export and compile the constructed surrogate model as a standalone executable code (where PSUADE offers C and Python choices). The executable code will then be used to perform function evaluations; passing in settings of $\theta_1 \ldots \theta_5$ will return the QoI as a scalar value.
4. Modify the C code for the exported surrogate model. The reason for this modification is that exported C code is structured to perform function evaluations, i.e., accept input and compute the QoI (i.e., filling shock location) as output. However, the optimization procedure used in deterministic calibration aims to find the set of model parameters that minimize the residual. That means the exported surrogate model code is modified to not only evaluate the QoI, but also to calculate the residual (Equation 7) by taking the difference of computed value ($S_i(\boldsymbol{\theta},\mathbf{x})$) and the corresponding experiment's QoI (y_i). If

this modification is not performed, the optimization will be attempted for the wrong objective.

5. Utilize Bound Optimization By Quadratic Approximation (BOBYQA) optimizer in PSUADE to perform an optimization to find the best set of $\theta_1 \ldots \theta_5$ values that give the least residual. See Appendix A for input files used for running the PSUADE optimizer. To explore all possible solutions, perform the optimization 10 or 15 times then assess which set of proposed settings are most common among the trials.

Table 2: Proposed Settings for the Modeling Parameters Obtained through Deterministic Calibration

θ_1 : Pressure Linear Scale Factor	θ_2 : Vol. Fraction Exponential Scale Factor	θ_3 : Statistical Weight	θ_4 : Vol. Fraction at Maximum Packing	θ_5 : Solid Slip Velocity Factor
14.309	2.165	12.241	0.399	0.828

Validation of the Proposed Calibrated Settings: The proposed calibrated model parameters potentially involve many sources of uncertainty. These doubts originate from model errors propagated through the surrogate model (modeling assumptions, simplifications, and approximations included with the introduction of a surrogate model instead of actual MFiX-PIC simulations) and data provided as input. For this case, no experimental error exists since an analytical solution provided the comparative dataset, but this is not the general case; care should always be taken in the validation process.

In order to assess the effectiveness of the proposed calibrated settings, a two-step process was employed for validation:

1. All 120 samples from the initial design of experiments were rerun with the proposed calibrated settings for $\theta_1 \ldots \theta_5$ and compared against the analytical solution obtained for the corresponding 120 samples, which enabled precise assessment of % Relative Error.
2. For a more rigorous assessment, 119 new samples were generated based on new $x1$:Initial Concentration settings in the range of 0.05 to 0.25. The new samples were checked to ensure these were totally unseen samples, i.e., the same $x1$ setting was not used in the previous 120 sample campaign. A new simulation campaign was carried out based on the 119 samples of $x1$ using the proposed calibrated model settings for each scenario outlined below as input to MFiX-PIC. The QoI derived from the simulation results were then compared against the analytical solution obtained for the corresponding 119 samples.

For each of the above validation campaigns, 6 scenarios were considered to better understand the effect of the proposed calibrated settings compared to default MFiX-PIC settings or those proposed in the V&V Manual (Vaidheeswaran et al., 2020):

(V.1) Employ MFiX-PIC default settings for all 5 model parameters.

(V.2) Employ proposed calibrated setting only for θ_5 and set the remaining 4 to default.

(V.3) Employ proposed calibrated settings for θ_5 and θ_4, then set the rest to default settings.

(V.4) Employ proposed calibrated settings for all 5 model parameters.

(V.5) Employ proposed calibrated settings for θ_5 and remaining settings from V&V manual proposed settings.

(V.6) Employ V&V manual proposed settings for all 5 model parameters.

In the cases above, default settings were determined by developers based on user experience. In fact, one of the major motivations of the current study is to verify if these values are sufficient to model the wide range of flow dynamics seen in industrial applications. In similar consideration, settings from the V&V manual (Vaidheeswaran et al., 2020) were also used.

These 6 scenarios were considered for the first validation campaign where the original 120 sample based simulation campaign was rerun. For the second validation step, all scenarios except V.3 were considered.

The proposed Scenarios V.1 through V.6, emerged as areas of interest based on both user and developer experiences to determine if hybrid combination of settings might provide any additional benefit.

Validation Step (1): Rerun of the original simulation campaign with 120 samples.

The intent of Validation Step (1) was to implement the calibrated model settings into the original 120 samples and compare the resulting QoI to equivalent analytical solutions. Then, Scenarios V.1–V.6 were further run to examine subsequent effects. While testing these scenarios, the same $x1$ settings obtained from the 120 sample campaign were used, but the 5 model parameter settings were based on the combinations for each scenario described above. For example, when running Scenario V.4, the proposed calibrated model settings from Table 2 were entered for each of the 120 samples while the $x1$ setting was changing based on the original campaign's settings.

Table 3 shows the settings used for scenarios V.1–V.6 in a tabulated format. Text coloring was used to facilitate easier review of how the blended scenarios were employed. For example, for scenario V.3 in the fourth column from left, blue colored numbers indicate settings originating from scenario V.1, and red colored numbers indicate settings originating from Scenario V.4. Also, preliminary descriptive statistics for the QoI, including average, minimum, and maximum of the % relative errors are provided at the bottom of each column. The % relative error figures reported indicate difference between analytical and simulation results for the QoI (y2: Location of filling shock) when settings for the model parameters are used under each scenario. Negative % relative error indicates under-prediction by MFiX-PIC whereas positive % relative error indicates over-prediction.

Scenario V.4 indicates that when the maximum % relative error from 120 samples is considered, the proposed calibrated settings are superior to default settings (13.24% versus 54.52%), and slightly inferior to the V&V manual suggested settings (13.24 % versus 10.87%). When minimum % relative error is considered, proposed calibrated settings performed better than the V&V manual suggested settings (-15.02 % versus -24.25 %), but worse than the default settings in an absolute sense (i.e., -15.02 % versus 8.83 %).

Table 3: Model Parameter Settings Employed for Each of the 6 Scenarios used in the First Validation Simulation Campaign

Scenarios:	(V.1)	(V.2)	(V.3)	(V.4)	(V.5)	(V.6)
MFIX-PIC Model Parameter	[1] Default	[2] Calibrated Setting only for θ_5 & Rest Default Settings	[3] Calibrated Setting only for θ_5 & θ_4, Rest Default	[4] Calibrated Settings for All (θ_1, θ_2, θ_3, θ_4, θ_5)	[5] Calibrated Setting only for θ_5 & Rest V&V Manual	[6] V&V Manual Settings
Theta1 (θ_1): Pressure linear scale factor	100	100	100	14.309	10	10
Theta2 (θ_2): Vol. fraction exponential scale factor	3.0	3.0	3.0	2.165	3.0	3.0
Theta3 (θ_3): Statistical weight	5.0	5.0	5.0	12.241	5.0	5.0
Theta4 (θ_4): Vol. fraction at maximum packing	0.42	0.42	0.399	0.399	0.4	0.4
Theta5 (θ_5): Solid slip velocity factor	1.0	0.828	0.828	0.828	0.828	0.5
avg	**23.67%**	**10.43%**	**7.21%**	**-0.19%**	**2.09%**	**-4.63%**
min	8.83%	-2.65%	-8.61%	-15.02%	-12.74%	-24.25%
max	54.52%	42.87%	32.12%	13.24%	19.62%	10.87%

When the average of all 120 samples is considered, Scenario V.4 further illustrates that the proposed calibrated settings appear to be the best performer with an average % relative error of -0.19% compared to 23.67% and -4.63%. However, the average-based comparison might be

misleading as over-prediction and under-prediction may cancel error effects. To better understand the characteristics of these relative errors, Figure 12 and Figure 13 are offered for further visualization.

Figure 12 compares errors at the sample level. Each bar, from left to right, represents an individual run and the resulting % relative error between the analytical value of the QoI, $y2$:Location of filling shock and the predicted value of $y2$. Blue represents the relative error results from Scenario V.1; red represents the relative error results from scenario V.4; and, green represents the relative error results from Scenario V.6. The remaining hybrid combination scenarios shown in Table 3 (V.2, V.3, and V.5) are not shown for the sake of brevity.

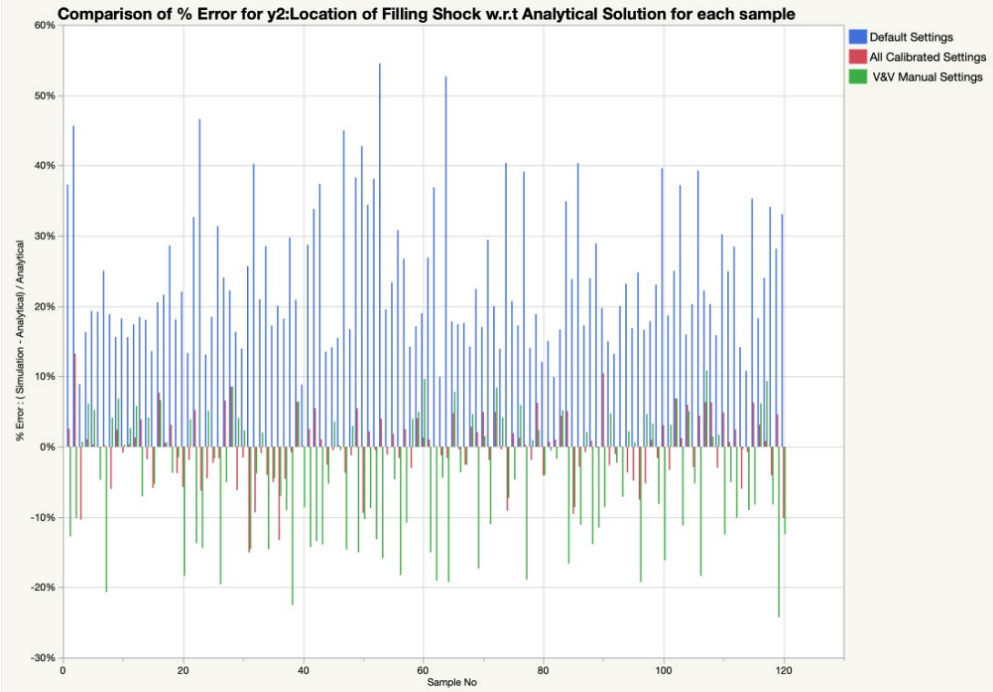

Figure 12: Comparison of % relative error for QoI (y_2:Location of Filling Shock) between Analytical Solution and V.1 (blue), V.4 (red), and V.6 (green).

Figure 12 indicates that Scenario V.1, which employed MFiX-PIC default settings, consistently over-predicted the location of the filling shock. It further indicates that Scenario V.4, which employed the calibrated settings, and Scenario V.6, which employed the V&V manual settings, resulted in a mix of over and under-prediction for the location of the filling shock.

Figure 13 offers a view of relative error between the 120 sample solutions and their associate analytical solutions in the form of histograms. In particular, the relative error of the QoI y2: location of filling shock, is examined for scenarios V.1–V.6. Ideally, the histogram should appear *normal* in a probabilistic sense with a mean of zero.

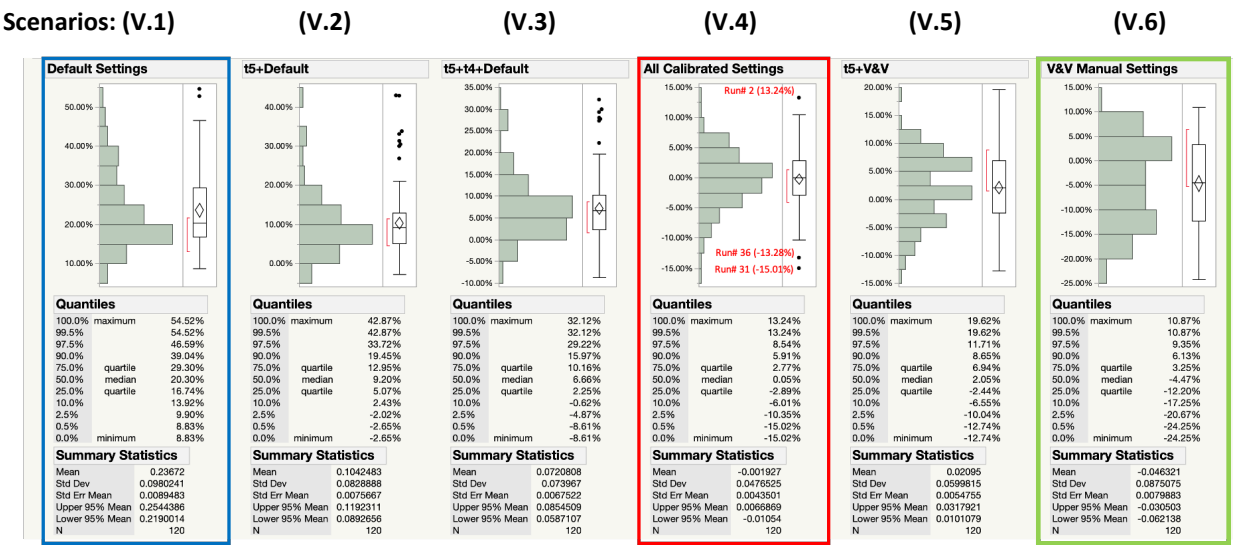

Figure 13: Comparison of % Relative Error for QoI (Location of Filling Shock) with respect to Analytical Solution for each sample from the original design of experiments runs.

Following the color scheme of Figure 12, Scenario V.1 (blue), Scenario V.4 (red), and Scenario V.6 (green), Figure 13 clearly illustrates the over-prediction noted in Scenario V.1. Where Scenarios V.4 and V.6 were described as having both over and under predictions, it is now more clear that Scenario V.4 has more *normal* relative error than Scenario V.6.

In particular, the % Relative Error histogram for Scenario V.1 clearly shows over-prediction since all of the samples show a positive sign on % Relative Error with a median of 20.3% error and a minimum of 8.83%. The distribution of relative errors also appears to be skewed with a maximum computed relative error of 54.52%. (Note that the numbers reported under the Summary Statistics section of Figure 13 are {% Relative Error / 100}. This is true for all similar subsequent figures.)

Relative error improves slightly for Scenario V.2 where the proposed calibrated setting for θ_5 (i.e., $\theta_5 = 0.828$) is implemented in cooperation with default settings for the remaining modeling parameters (i.e., $\theta_1 = 100$, $\theta_2 = 3.0$, $\theta_3 = 5$, $\theta_4 = 0.42$). The figure indicates that the median error percentage shifted from 20.3% to 9.20% and few samples show negative relative error percentages indicating under-prediction. Note that the overall data skew still trends towards maximum relative error, and there are outliers, shown as full black circles in the box plot section on the right side of each column.

In Scenario V.3, where θ_4 and θ_5 were set based on the proposed calibrated settings and θ_1, θ_2 and θ_3 were default settings, the median relative error percentage slightly improves to 6.66 %. Also, relative errors are more evenly distributed, particularly when outliers are disregarded.

Scenario V.4 employed all of the proposed calibrated model settings and displays an almost normal distribution centered around 0.0%, which is also the median relative error. Three outlier samples have been identified and indicated in the figure. Among these, Run #2 was determined to have one of the settings ($x_1 = 0.2457$) close to the maximum in the parameter range considered (i.e. $x_1 \leq 0.25$). This could be associated with the outlier behavior observed, as x_1 was

identified as the most influential parameter on the QoI. However, the remaining outliers require further investigation (i.e., Run #36, and #31, shown in red in Figure 13 under V.4 Scenario). A preliminary investigation has been launched to expose some of the critical MFiX-PIC variables. This will enable further analysis and may determine whether the issue originates from the switching algorithm discussed in the last paragraph on page 6.

Scenario V.5 used the proposed calibrated setting for θ_5 and the remaining model parameters were set as suggested in the V&V manual (Vaidheeswaran et al., 2020). The relative errors display a bi-modal distribution with maximum relative error around 20% (over-prediction) and 12.74% (under-prediction).

Finally, Scenario V.6 employed settings recommended after initial validation studies (Vaidheeswaran et al., 2020) for all 5 model parameters. The relative errors appear to be spread evenly between 10.0% and -20.0%, which is quantitatively worse than Scenario V.4.

After comparing all of the scenarios, it is clear that Scenario V.4, which employed the proposed calibrated model settings for all 5 parameters, gave the most desirable relative error distribution. If the 3 outliers identified can be disregarded, the maximum relative error is capped around 10% with a mean and median at 0.0%.

Figure 14 further investigates the relative error seen in Scenarios V.1 through V.6, . The figure is identical to Figure 13 *except* an additional highlighting is offered for consideration. Shown as a dark hatched pattern, these areas represent samples that produced error between 2.5% and +2.5% in Scenario V.4.

This visual approach allows the user to consider the relative error of similar samples across different scenarios, as well as the total number of samples within the error band. For example, using the 5% relative error range that was achieved with the proposed calibrated model parameters of Scenario V.4 as a basis, note the wider relative error range of other scenarios, such as +10% to -25% in Scenario V.6. Also note that by examining only the Scenario V.4 histogram, the error band represented incorporates almost half of all samples.

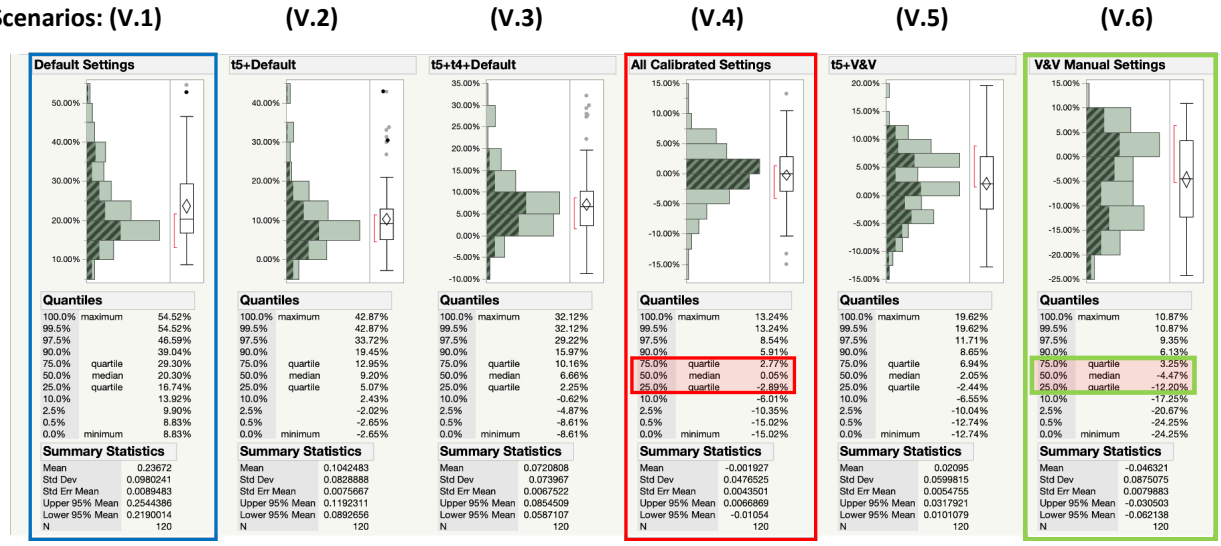

Figure 14: Comparison of % Relative Error for QoI (Location of Filling Shock) with respect to Analytical Solution for each sample from the original design of experiments runs with median and 50% range values highlighted.

Validation Step (2): A new simulation campaign for a set of 119 unseen samples.

In the second phase of validation for the proposed calibrated settings, a more rigorous approach was employed. For 5 of the scenarios presented in Table 3 (V.1, V.2, V.4, V.5, V.6), MFiX-PIC simulations were conducted where x_1 : Velocity at Inlet was set to 119 new and unique settings on the interval $[0.05,0.25]$. These new values for x_1 represent velocities associated with the midpoints of successive initial solids concentration settings from the 120 samples originally generated using OLH sampling (Figure 7). Analytical solutions for the new 119 samples were then computed and used in the assessment of % Relative Error, which is the measure applied to determine the effectiveness of the calibration.

Table 4 shows the 5 scenarios employed for Validation Step (2). Similar to Table 3, blue and red text indicate similar values, and blue, red, and green outlines correspond to Scenarios V.1, V.4, and V.6. Note that Scenario V.3 was dropped in this new analysis when Validation Step (1) discounted its value.

Figure 15 compares % relative error at the sample level. Each bar, from left to right, represents an individual run and the resulting relative error between the analytical value of the QoI, $y2$:Location of filling shock and the predicted value of $y2$. Blue represents the relative error results from Scenario V.1; red represents the relative error results from Scenario V.4; and, green represents the relative error results from Scenario V.6. The remaining hybrid combination scenarios shown in Table 3 (V.2 and V.5) are not shown for the sake of brevity.

As in Validation Step (1), Scenario V.1 (the default MFiX-PIC settings) reveals over-prediction. And, Scenarios V.4 (calibrated settings) and V.6 (V&V Manual settings) reveal a mixture of over and under-prediction.

Table 4: Settings Employed for Each of the 5 Scenarios used in the Second Validation Simulation Campaign with Unseen Samples

Scenarios:	(V.1)	(V.2)	(V.4)	(V.5)	(V.6)
MFiX-PIC Model Parameter	**[1] Default**	**[2] Calibrated Setting only for θ_5 & Rest Default Settings**	**[4] Calibrated Settings for All (θ_1, θ_2, θ_3, θ_4, θ_5)**	**[5] Calibrated Setting only for θ_5 & Rest V&V Manual**	**[6] V&V Manual Settings**
Theta1 (θ_1): Pressure linear scale factor	100	100	14.309	**10**	**10**
Theta2 (θ_2): Vol. fraction exponential scale factor	3.0	3.0	2.165	3.0	3.0
Theta3 (θ_3): Statistical weight	5.0	5.0	12.241	5.0	5.0
Theta4 (θ_4): Vol. fraction at maximum packing	0.42	0.42	0.399	**0.4**	**0.4**
Theta5 (θ_5): Solid slip velocity factor	1.0	0.828	0.828	0.828	**0.5**
avg	**22.99%**	**-3.80%**	**-0.96%**	**2.09%**	**-5.51%**
min	5.62%	-27.44%	-15.69%	-17.15%	-27.44%
max	45.45%	17.23%	17.73%	15.84%	10.06%

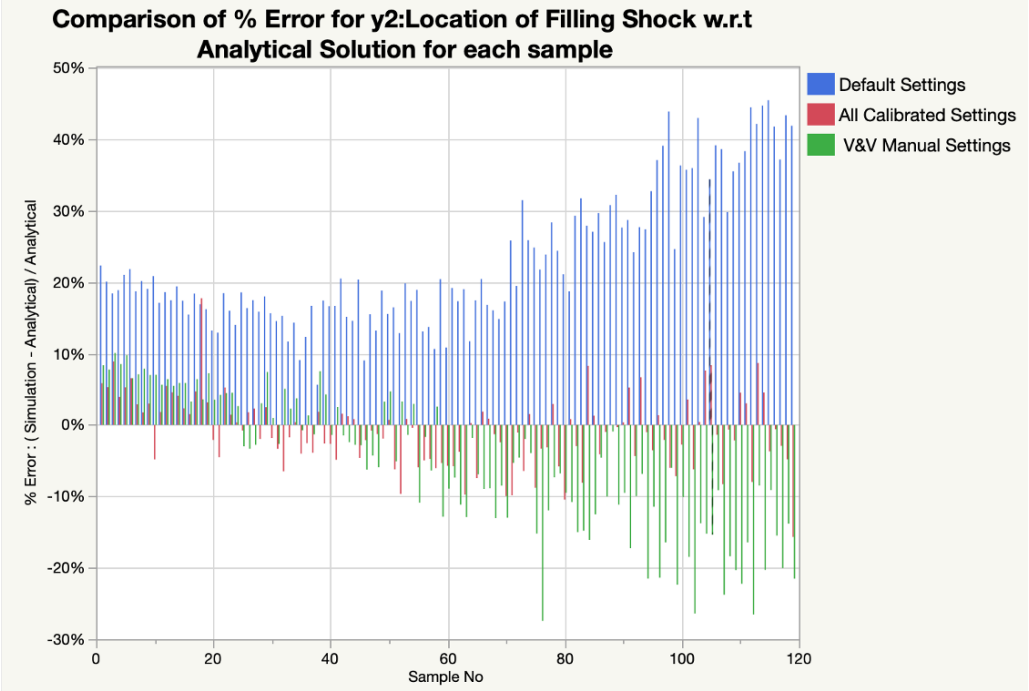

Figure 15: Comparison of % Relative Error for QoI (Location of Filling Shock) with respect to analytical solution for each sample from the unseen test runs.

Figure 16 offers a view of relative error between the 119 sample solutions and their associate analytical solutions in the form of histograms. In particular, the relative error of the quantity of interest, y2: location of filling shock, is examined for the same scenarios presented in Table 4.

Two potential outliers (Run #119 and #18) are highlighted in red for Scenario V.4 in Figure 16. If these outliers are excluded, the % Relative Error histogram shows an almost normal distribution between 10.0% and -12.5%, with a median around -1.0% error. When compared with the other scenarios, the proposed calibrated settings (Scenario V.4) offer a significantly narrower relative error distribution. The preliminary investigation launched for the potential outliers identified in Figure 13 is expected to provide additional insight whether the same root cause is applicable for the observed outlier behavior.

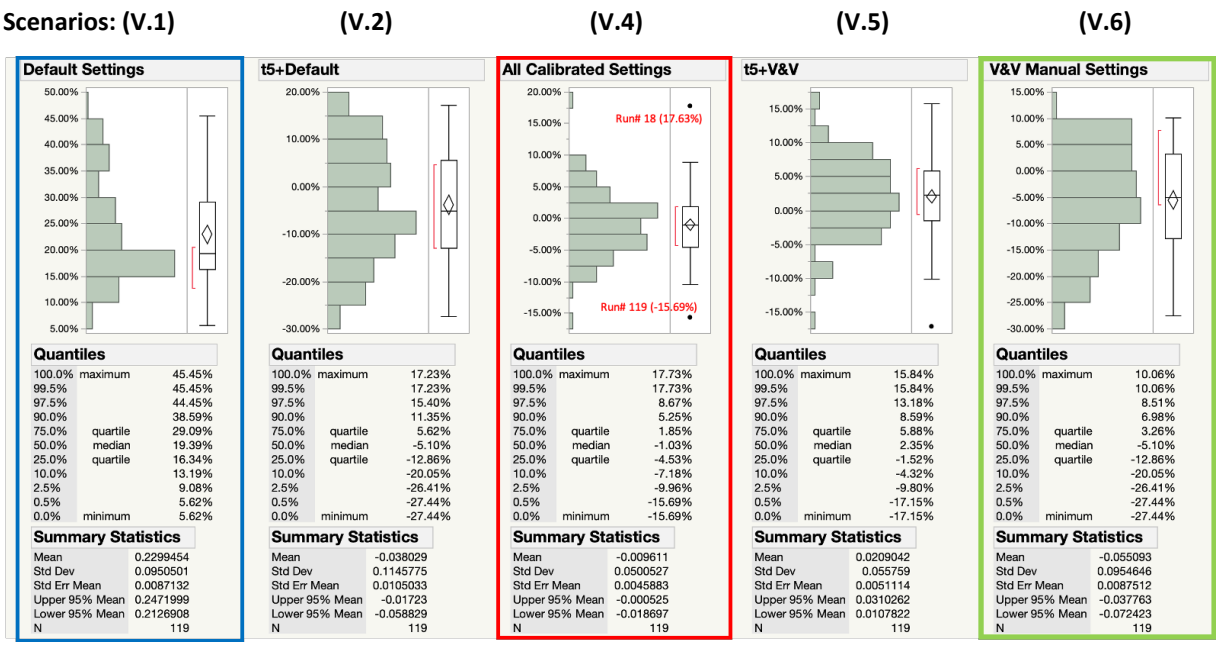

Figure 16: Comparison of % Relative Error for QoI (Location of Filling Shock) with respect to analytical solution for each sample for the unseen 119 samples.

Figure 17 further investigates the relative errors seen in the current scenarios. The figure is identical to Figure 16 *except* an additional highlighting is offered for consideration. Shown as a dark hatched pattern, these areas represent samples that produced error between -2.5% and +2.5% in Scenario V.4.

This visual approach allows the user to consider the error of similar samples across different scenarios, as well as the quantity of samples within the error band. For example, using the 5% error range that was achieved with the proposed calibrated model parameters of Scenario V.4 as a basis, note the wider relative error range of other scenarios, such as +10% to - 25% in Scenario V.6. Also note that by examining only the Scenario V.4 histogram, the relative error band represented incorporates almost half of all samples. In particular, 50% of 119 samples reside within 1.85% to -4.53% relative error range for Scenario V.4, whereas the same 50% reside between 3.26% and -12.86% in Scenario V.6.

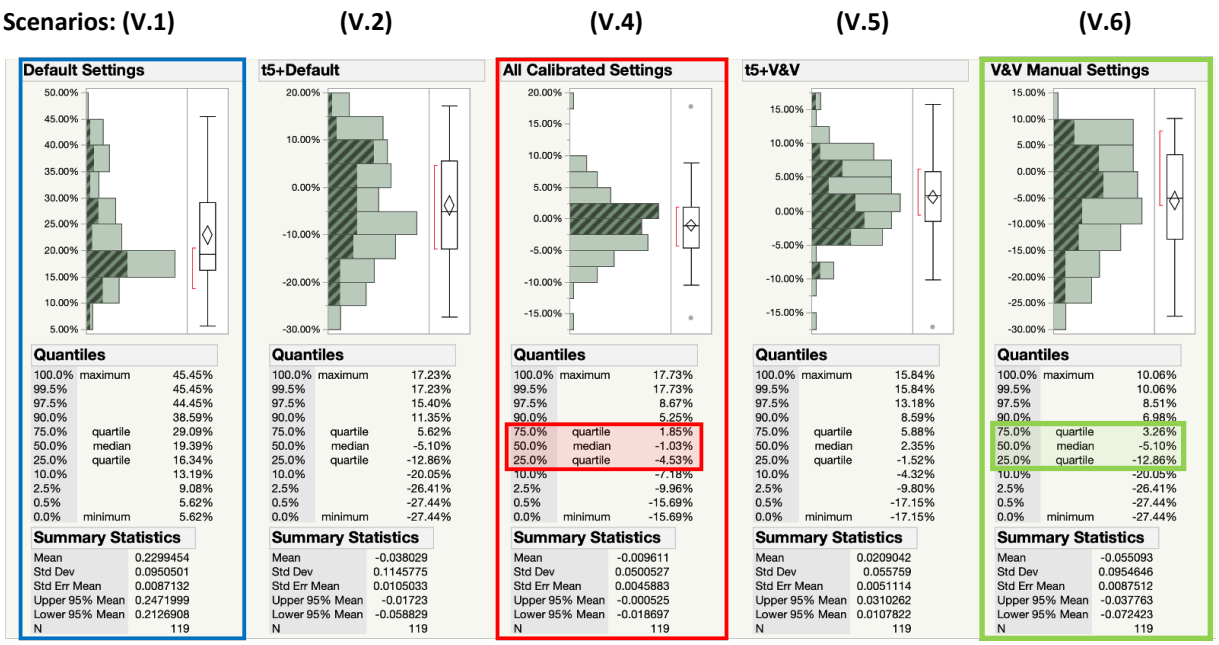

Figure 17: Comparison of % Relative Error for QoI (Location of Filling Shock) with respect to analytical solution for each sample for the unseen 119 samples with median and 50% range values highlighted.

Assessment of the Effect of Experimental Sample Size: As discussed earlier, 120 samples of MFiX-PIC simulations were performed to construct a surrogate model to characterize the relationship among 6 input parameters ($\theta_1,\theta_2,\theta_3,\theta_4,\theta_5,x_1$) and 1 QoI ($y2$). Following, another dataset with 21 samples was generated for the same QoI by computing the analytical solution at 21 different x_1 settings using Equation 5. This dataset with 21 samples was used in lieu of experimental data required for deterministic calibration. Then, the calibration process required minimization of the residual shown in Equation 7, which necessitates the use of the surrogate model to evaluate $S_i(\boldsymbol{\theta},x)$ at each i for $i = 1,21$.

A separate study was carried out to better understand the effect of experimental data sample size, i.e., instead of a 21 sample based analytical solution dataset, the question, "how would an 11 sample or 5 sample based dataset affect the deterministic calibration results?" was investigated.

A visual illustration of the original 21 sample dataset can be seen in Figure 18. The 21 sample group is shown with blue cross symbols. Note that the same figure contains the illustration of two additional datasets generated for this assessment, one with 11 evenly spaced samples (shown with red circle symbols) and one with 5 evenly spaced samples (shown with green diamond symbols). The spacing may cause some of the sample markers to overlap. The new analytical solution datasets were generated by keeping the same lower and upper bounds of x_1 while reducing the intermediate sample locations uniformly.

Note that the analytical solution is being used as if the results were coming from experiments without any noise, and the same surrogate model constructed from the 120 sample simulation campaign was used in this sensitivity assessment.

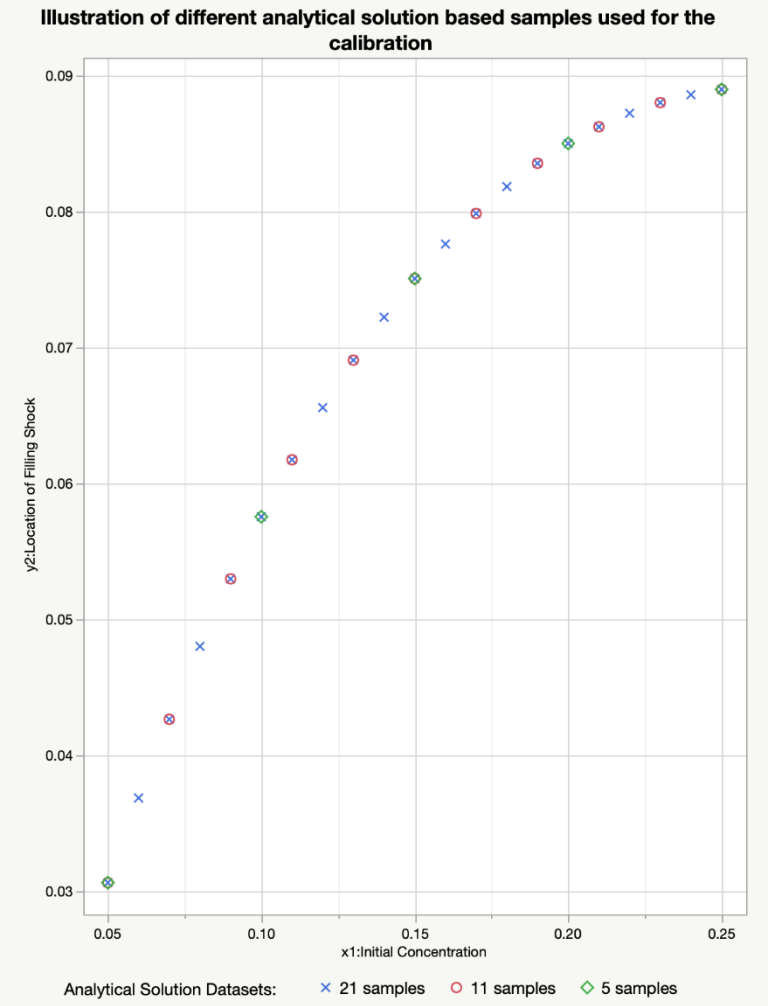

Figure 18: Three different analytical solution samples (5, 11, and 21 samples) used to assess the sensitivity of deterministic calibration results.

To perform validation of the new proposed calibrated settings based on 5 and 11 samples of the analytical solution, the following five cases were considered:

(C.1) Default settings of MFiX-PIC (first histogram from the left).

(C.2) Obtained by employing 21 samples of the analytical solution during the minimization of residuals (second histogram from the left with a column label of ”All Calibrated w Exp_n21”).

(C.3) Obtained by employing 11 samples of the analytical solution during the minimization of residuals (third histogram from the left with a column label of ”All Calibrated wExp_n11”).

(C.4) Obtained by employing 5 samples of the analytical solution during the minimization of residuals (fourth histogram from the left with a column label of ”All Calibrated wExp_n5”).

(C.5) V&V manual based (last histogram from the right).

Validation simulations were then performed for the unseen 119 samples with the new calibrated model parameter settings for cases C.3 and C.4. Figure 19 shows the comparison of the % Relative Error histograms for the five cases considered to assess the sensitivity of the analytical solution sample size.

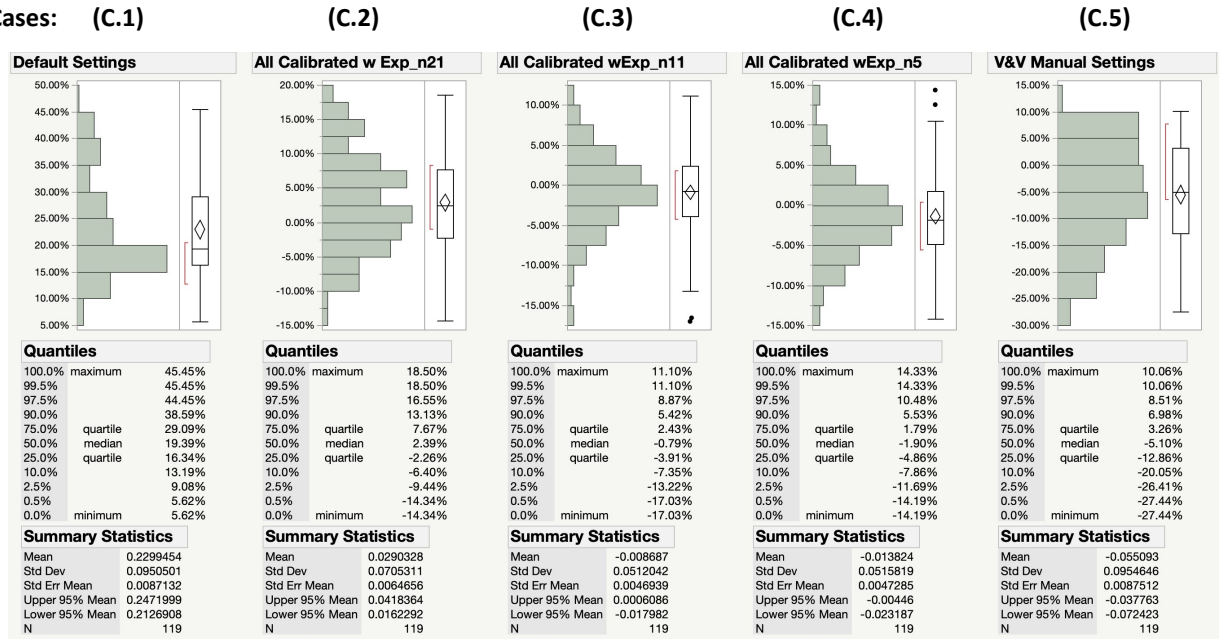

Figure 19: Comparison of % Relative Error for QoI (Location of Filling Shock) for the proposed settings of model parameters calibrated with varying size of analytical solution based data sample size (i.e., 21, 11, and 5).

Among the C.1 through C.5 cases, case C.3, based on calibrated settings from 11 samples, appeared to give the best results with the least amount of relative error as compared to other cases. Maximum relative error was 11.1% and minimum relative error was -17.03%. The mean relative error over the 119 sample campaign was -0.88%. The next best was case C.4, based on calibrated settings from 5 samples.

To further understand the effect of sample location, an additional assessment where a non-uniform selection of x_1 over the range $[0.05, 0.25]$ was made. Figure 20 shows a comparison of the original 11 uniformly distributed samples (red colored circle symbols) and the 11 non-uniformly distributed (purple colored plus symbols) dataset employed for calibration sensitivity assessment. As seen from the figure, the non-uniform sample set does not have samples residing at the boundaries of the $[0.05, 0.25]$ interval for x_1 but have two nearly adjoint samples very close around x_1 around 0.06 and similar two samples in the upper end. Both datasets only overlap at $x_1 = \{0.09, 0.15, 0.19\}$. The motivation for this investigation was to assess the effect of sparse data, which is typically encountered with physical experiments.

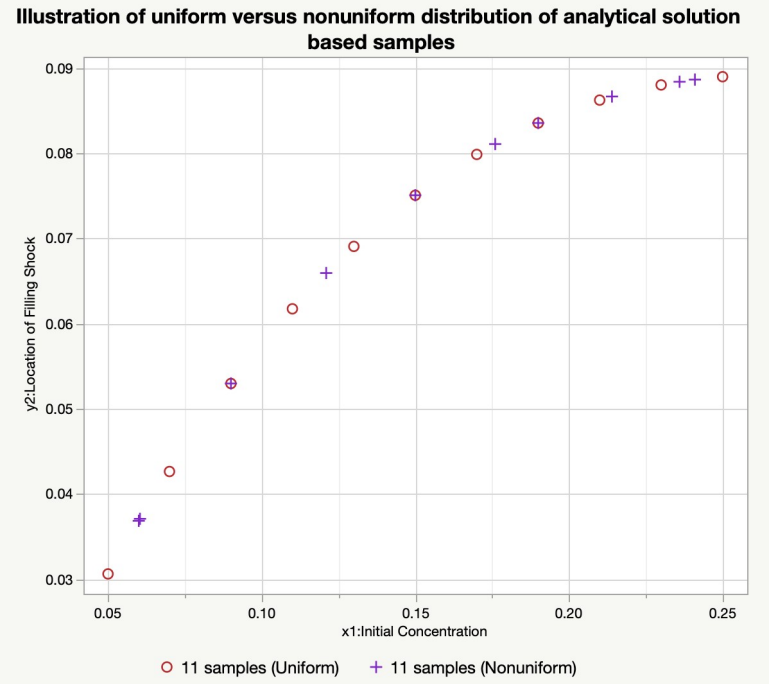

Figure 20: Uniform versus non-uniform distribution of the 11 sample analytical solution dataset to assess the sensitivity of deterministic calibration results.

Figure 21 offers a histogram view of % relative error for cases C.1 through C.5 with uniform spacing, and case C.3 with non-uniform spacing. In particular, the % relative error of the quantity of interest, y2: location of filling shock, is examined to assess the sensitivity of the deterministic calibration procedure employed to the experimental data sample size and the uniformity of the experimental sample distribution. Recall that an analytical solution was used in lieu of experimental data.

A direct comparison of cases C.3 with uniform and non-uniform sample spacing reveals similar lower error bounds but disparate upper error bounds, with non-uniform spacing showing a roughly 1.25% lower relative error. Figure 20 shows that case C.3 with non-uniform spacing has two samples very close to the upper bound of x_1, which might be a plausible explanation for why the upper bound of % Relative Error is less. In particular, the two samples are closer to each other and are within the proximity of the x_1 upper bound value as opposed to a single sample at the upper bound limit. Additionally, when inspected closely, the relative errors exceeding 10% were attributed to samples # 111 and # 116, which had x_1 values of 0.23527 and 0.24348, respectively. Overall, there is a pronounced shift in the median but not mean % Relative Error, which suggests the deterministic calibration results appear to be robust for non-uniform sampling.

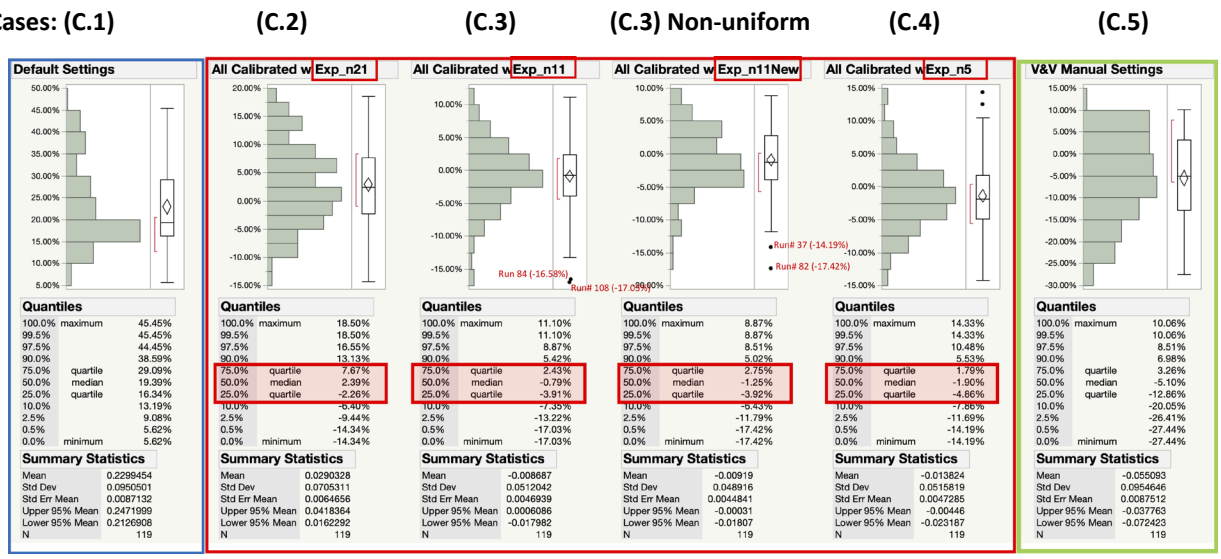

Figure 21: Comparison of % Relative Error for QoI for the proposed settings of model parameters calibrated with varying size of analytical solution based data sample size (i.e., 21, 11, and 5) and non-uniform 11 sample case.

Deterministic Calibration Results with Nodeworks:

In this section, the calibration results obtained with Nodeworks are presented and compared to the analytical solution.

Figures 22 and 23 illustrate workflows developed for deterministic calibration within Nodeworks. The *Residual Function* node (shown as the center step in Figures 22 and 23) was created particularly for this study and follows the logic of Equation 7. Other nodes shown were already available within the standard Nodeworks framework.

Each node performs a specific task. In Figure 22, the leftmost node, *Response Surface* (RS), uses the surrogate model to perform functional evaluations for the QoI, in lieu of running MFiX simulations. This is accomplished by importing a tabular dataset that includes (θ_1, θ_2, θ_3, θ_4, θ_5, and $x1$) as input. The rightmost node, *General Optimizer* (GO), solves the minimization problem and works cooperatively with the user-defined Residual Function. Within the RS node, the Error tab (highlighted in blue) reveals a cross-validation results graph of the Gaussian Process Model based data-fitted surrogate model. When analytical results align with model results well (along the line), this is one indicator of good fit. Additional evaluations of RMSE and error histogram visualization (available under Plots) further assist in the determination of model quality.

Figure 23 reveals a comparison plot of different surrogate models fitted based upon the RMSE metric. This bar-chart is available under the Compare tab of the RS node. For consistency with earlier PSUADE results, the Gaussian Process Model was chosen for this study. The parallel coordinates plot shown under the Parallel Plot tab of the GO node gives proposed values for (θ_1, θ_2, θ_3, θ_4, θ_5) after optimization. The user controls the number of attempts to optimize, and similar values for the proposed values are highlighted by Nodeworks.

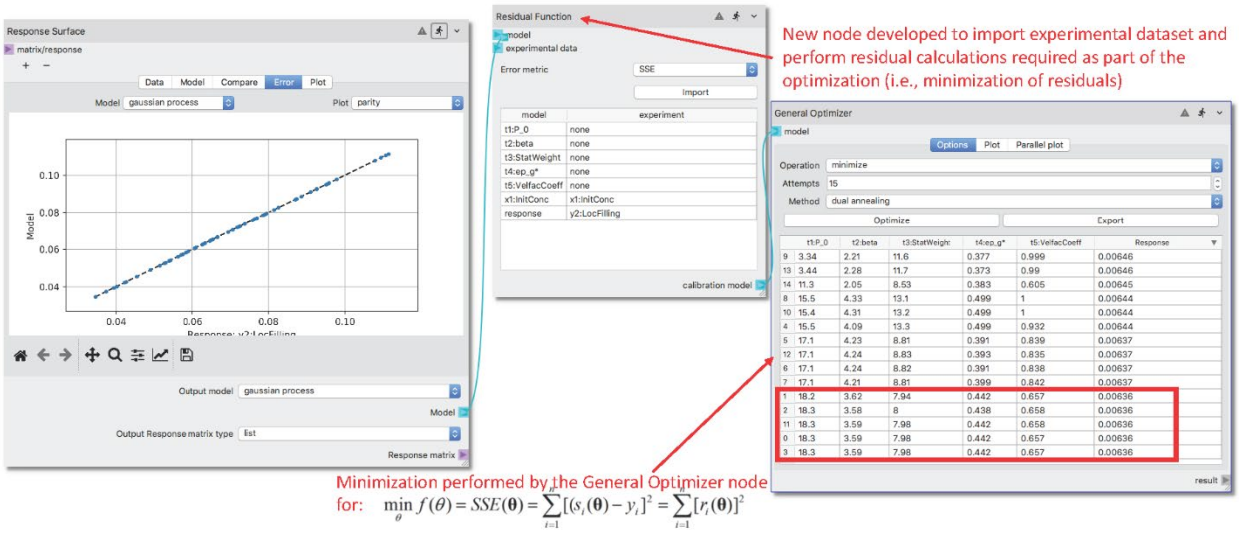

Figure 22: Nodeworks workflow for deterministic calibration view #1 showing the cross validation errors for the data-fitted surrogate model (the node shown on the most left) and the tabulated results of the deterministic calibration as a result of 15 attempts (the node shown on the most right).

Table 5 compares the proposed settings for the input parameters (θ_1, θ_2, θ_3, θ_4, θ_5) from PSUADE and Nodeworks studies. The differences observed between the two UQ software's model parameter calibration results may originate from the differences in how surrogate model methodology has been implemented (e.g., both UQ toolkits offer Gaussian Process Model based surrogate model methodology but as two different implementations, and the global optimization algorithms employed were different). Nodeworks calibration results were evaluated using the same approach as PSUADE calibration results.

Table 5: Comparison of the Proposed Calibrated Model Parameters Based on PSUADE and Nodeworks Studies

MFiX-PIC Model Parameter	PSUADE Calibrated Settings for All (θ_1), θ_2, θ_3, θ_4, θ_5)	Nodeworks* Calibrated Settings for all (θ_1), θ_2, θ_3, θ_4, θ_5)	% Difference w.r.t. PSUADE Results
Theta1 (θ_1): Pressure linear scale factor	**14.309**	**18.300**	**27.9 %**
Theta2 (θ_2): Vol. fraction exponential scale factor	**2.165**	**3.590**	**65.8 %**
Theta3 (θ_3): Statistical weight	**12.241**	**7.980**	**-34.8 %**
Theta4 (θ_4): Vol. fraction at maximum packing	**0.399**	**0.442**	**10.8 %**
Theta5 (θ_5): Solid slip velocity factor	**0.828**	**0.658**	**-20.5 %**

Figure 24 shows a histogram plot of % Relative Error similar to Figure 16 except the validation test results are now based on Nodeworks calibrated model parameters. The same 5 scenarios are considered for comparison. Scenario V.4, which is based on the use of all 5 calibrated model parameters proposed by Nodeworks calibration study, appears to exhibit the best error distribution compared to other scenarios including V.6, which is based on V&V manual settings.

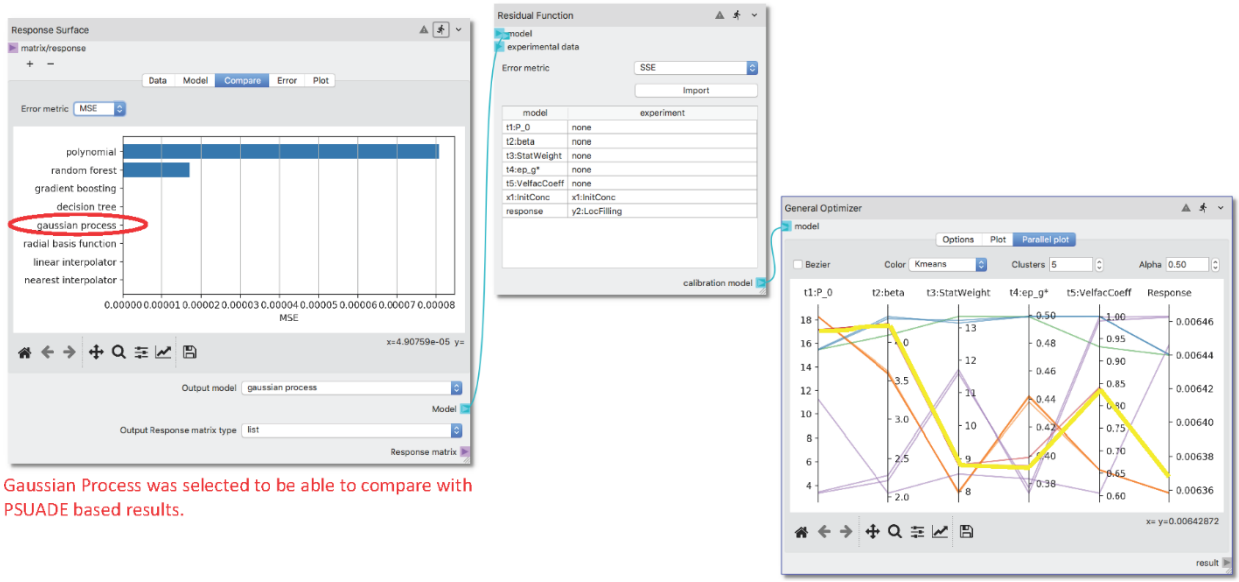

Gaussian Process was selected to be able to compare with PSUADE based results.

Figure 23: Nodeworks workflow for deterministic calibration view #2 showing the parallel coordinates plot of the result.

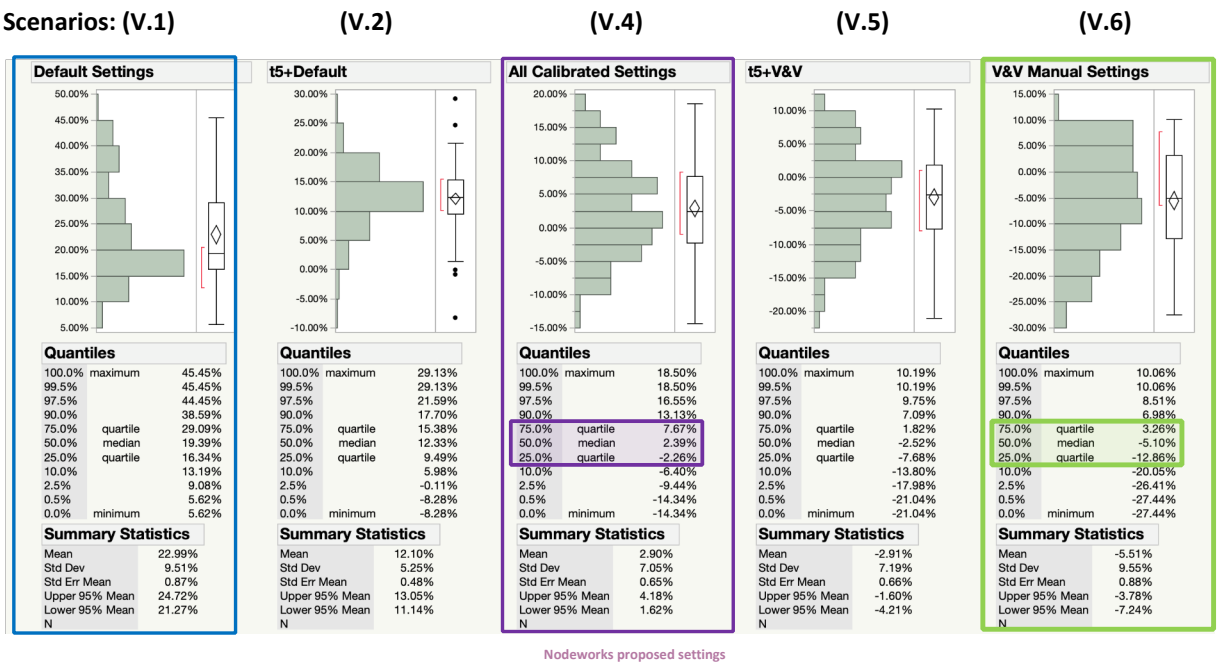

Figure 24: Comparison of % Relative Error histogram for QoI (Location of Filling Shock) with respect to Analytical Solution for the unseen 119 samples based on the proposed calibrated settings from Nodeworks.

Figure 25 shows a comparison of the % relative error histograms for the unseen 119 samples between scenario V.4 PSUADE-based and scenario V.4 Nodeworks-based calibrated model parameters. The histograms generated from scenarios V.1 and V.6 are also included for comparison as illustrated in earlier similar plots. The % relative error histogram obtained from PSUADE appears to have a narrower distribution compared to Nodeworks based results. Mean % relative errors were -1.03 % and 2.39 % for PSUADE-based and Nodeworks-based settings, respectively. In general, PSUADE-based results appear relatively better than Nodeworks-based results. However, both sets of results exhibited substantially better distribution of errors compared to Scenarios V.1 and V.6, which suggests that deterministic calibration performed with PSUADE and Nodeworks improved the results for this application.

To further investigate the error seen in the current scenarios, Figures 26 and 27 are offered. Both are identical to Figure 25 *except* an additional highlighting is given for consideration. Shown as a dark hatched pattern, these areas represent samples that produced relative error between -2.5% and +2.5% in Scenario V.4. In Figure 26, the hatching corresponds to PSUADE results, and in Figure 27, the hatching corresponds to Nodeworks results.

Comparing the two figures reveals differences in what samples produce particular error quantities. PSUADE captures 47 samples in this error band. Nodeworks captures only 32.

As PSUADE-based results capture more samples within ±2.5 % relative error interval, it can be concluded that for the given dataset and application, PSUADE-based deterministic calibration performed relatively better when compared to Nodeworks-based deterministic calibration. However, it is important to note that both UQ toolkits employ different surrogate model method implementation even if the same surrogate model method has been used. Also, two different

optimization algorithms were employed during this study, which might have contributed to the difference observed. A separate study with identical comparisons using the same surrogate model implementation and optimization algorithm would determine which method is truly superior.

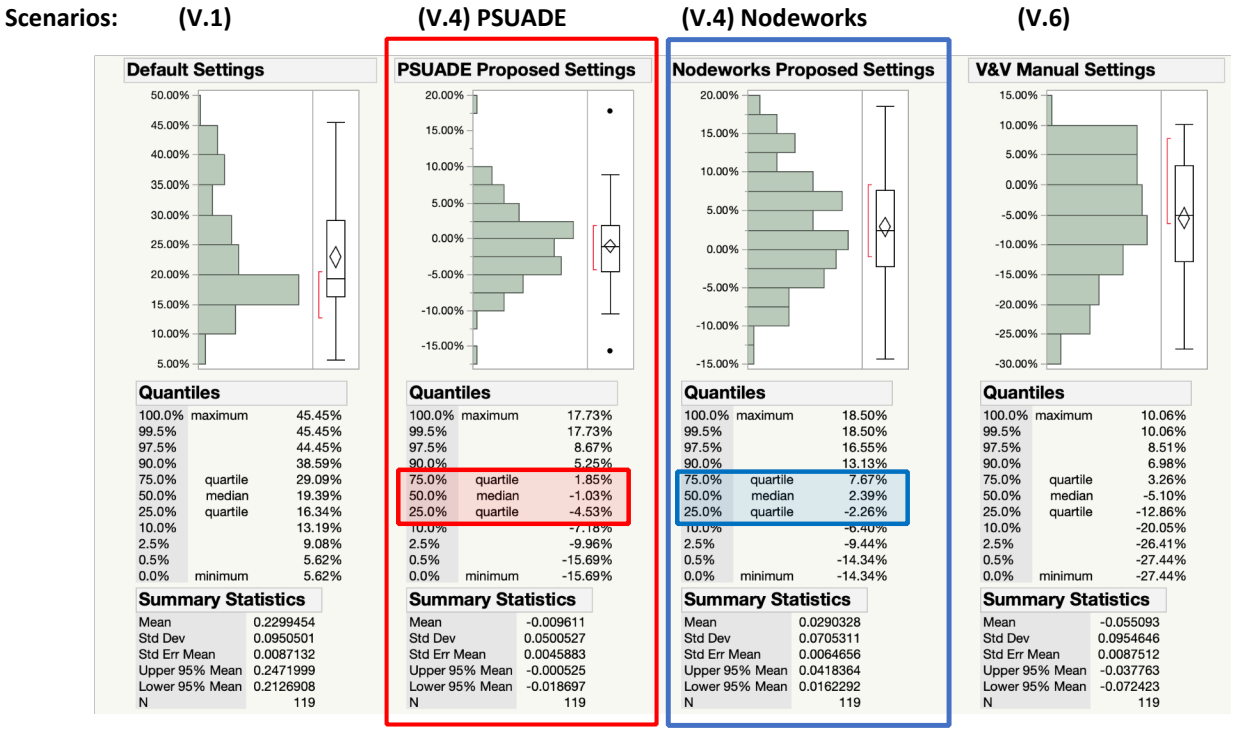

Figure 25: Comparison of % error histogram for QoI (Location of Filling Shock) with respect to Analytical Solution for the unseen 119 samples based on the proposed calibrated settings from PSUADE and Nodeworks

Scenarios: **(V.1)** **(V.4) PSUADE** **(V.4) Nodeworks** **(V.6)**

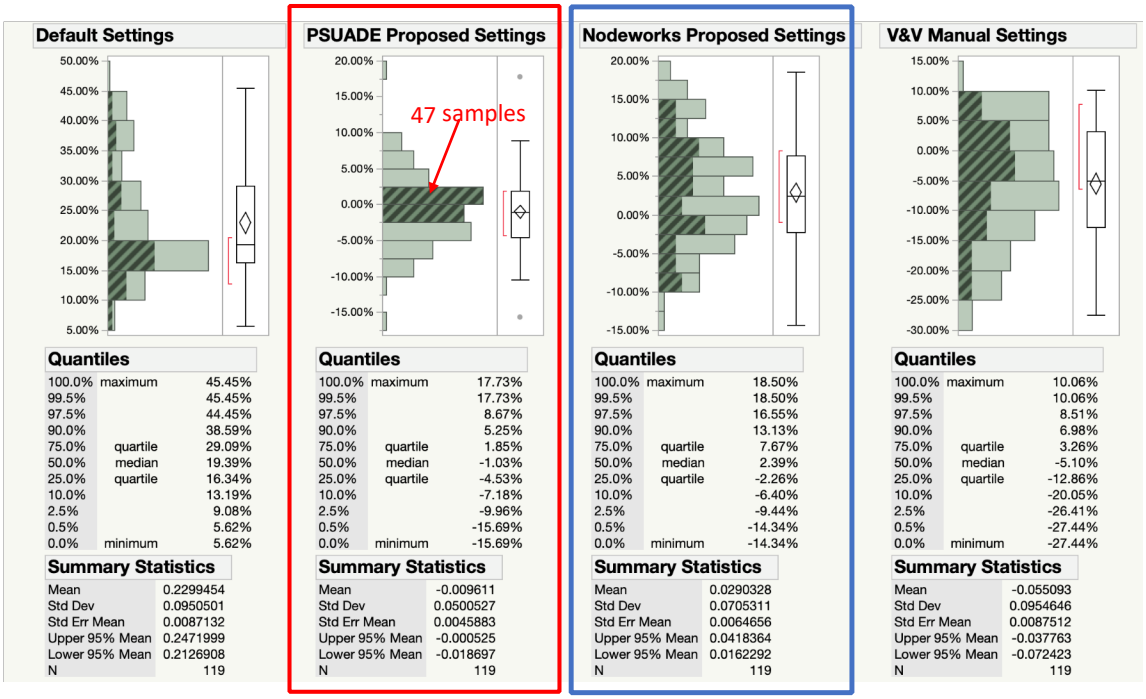

Figure 26: Comparison of % Relative Error histogram for QoI (Location of Filling Shock) for the unseen 119 samples where samples within ±2.5% error interval for PSUADE based calibrated settings are highlighted.

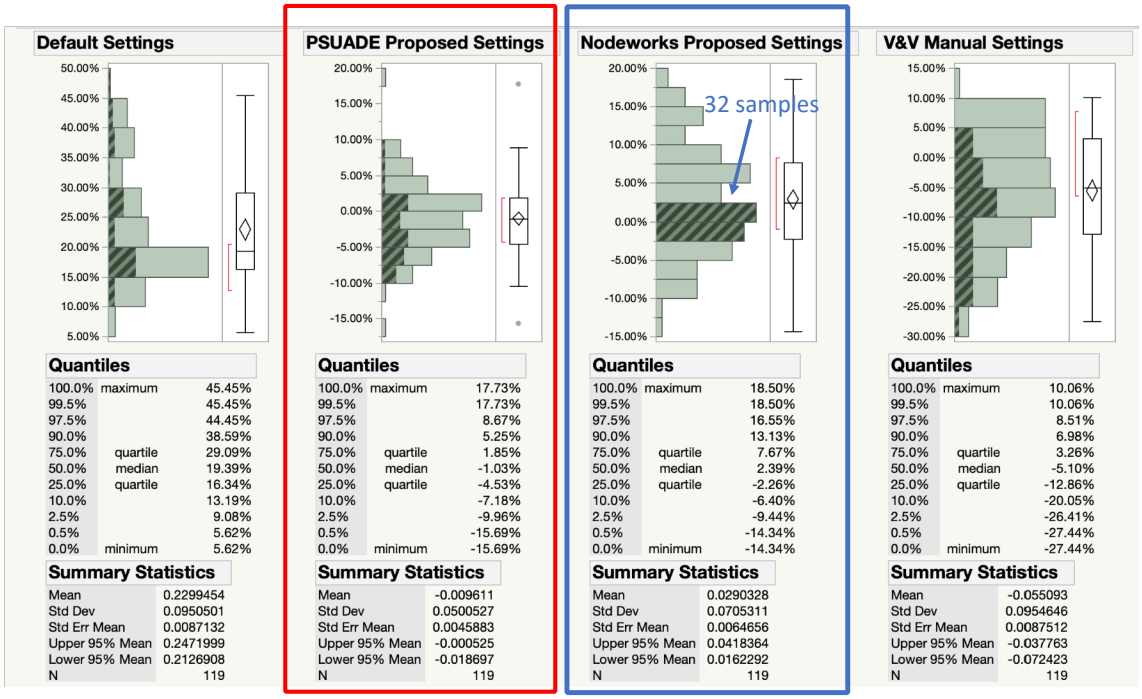

Figure 27: Comparison of % Relative Error histogram for QoI (Location of Filling Shock) for the unseen 119 samples where samples within ±2:5% error interval for Nodeworks-based calibrated settings are highlighted.

5. CONCLUSIONS

The study presented in this report evolved from systematic Verification, Validation and Uncertainty Quantification efforts initiated at the U.S. DOE's NETL to assess the credibility of the MFiX suite of solvers. This report follows two earlier reports related to (1) Verification and Validation of MFiX-PIC (Vaidheeswaran et al., 2020) and (2) Sensitivity Analysis of MFiX-PIC (Vaidheeswaran et al., 2021). The first study aimed to capture and document any discrepancy noted in MFiX-PIC by comparing simulation results to available experimental data directly. The second study aimed to evaluate the sensitivity of keyword-accessible modeling input parameters employed in MFiX-PIC, by examining several QoI as modeling input parameters varied.

The primary focus of this study was to develop and demonstrate a procedural methodology for improving the credibility of MFiX-PIC simulations by applying deterministic calibration methods to the modeling parameters considered. Three targeted applications were selected to encompass widely encountered flow configurations: particle settling, fluidized bed and circulating fluidized bed. This report documents the deterministic calibration of 5 MFiX-PIC modeling parameters in the context of the first targeted application, particle settling. A unique advantage for this problem is an analytical solution for the QoI, location of the filling shock. This enabled the calibration study to proceed without any physical experiments.

A dataset with 21 samples based on the analytical solution for the location of the filling shock was generated by varying the initial solids concentration parameter (x_1) within the interval $[0.05, 0.25]$. Then this dataset was used like observations from an experiment. However, no experimental uncertainty was considered for this calibration study.

The deterministic calibration procedure can be framed as the minimization of residuals (simulation - experiment) problem. In order to perform the thousands of evaluations required while testing different model parameter settings during optimization, a data-fitted surrogate model was constructed. This model, after assessing its quality for characterizing the relationship between input and output datasets, was then used instead of actual MFiX-PIC simulations to save time. Note that running thousands of MFiX-PIC simulations as part of an optimization loop would be prohibitively time-consuming.

A simulation campaign with 120 samples of actual MFiX-PIC simulations was designed using the Optimal Latin Hypercube sampling method for the 6 input parameters considered in Table 1. The settings used for the 6 input parameters and the QoI from the simulation campaign results were compiled in a tabular formatted ASCII file to be used as input to UQ toolkit software for constructing a surrogate model and for performing the remainder of the analysis.

Two separate UQ software, PSUADE from Lawrence Livermore National Laboratory (Tong, 2020) and Nodeworks developed at the NETL (NETL, 2020), were employed for data-fitted surrogate model construction. In addition, these software were used to conduct quality checks of the formed surrogate models and for performing the minimization of residuals to obtain the best set of model parameter settings. Although the same input dataset was imported to both software, some differences were observed in the resulting calibrated model settings. These differences are most likely related to the optimization algorithms unique to each software.

The effectiveness of the proposed calibrated model parameter settings obtained as a result of the deterministic calibration process was evaluated by running additional MFiX-PIC simulations using the new settings for model parameters (θ_1, θ_2, θ_3, θ_4, θ_5) and then calculating % relative

error with respect to the analytical solution for the location of the filling shock at the corresponding x_1 settings. In addition, a new set of simulations was performed at the same x_1 settings using both the default MFiX-PIC settings and those proposed in the V&V Manual for the 5 model parameters ($\theta_1,\theta_2,\theta_3,\theta_4,\theta_5$). An overall comparison of % relative error from each simulation was presented as well as a histogram view of % relative errors. Note that the availability of an analytical solution enabled performing an error assessment for each sampling simulation. This action is typically not feasible when physical experiments are utilized for the calibration process.

The proposed calibrated model parameter settings obtained with PSUADE UQ software were superior to the default MFiX-PIC settings and the settings proposed in the V&V Manual. The % relative error histogram plots for the proposed calibrated model parameter settings were demonstrated to yield substantially more accurate MFiX-PIC results for the particle settling application. This was shown in two steps. First, the original simulation campaign with 120 samples, which was used to construct the surrogate model were rerun and % relative error was calculated for each sampling simulation (Figure 13). Then, a more rigorous approach utilized 119 unseen samples of x_1 settings. Again, PSUADE-based proposed calibrated settings outperformed the other settings for the 5 model parameters in both validation steps as clearly seen in Figures 13 and 16.

Additionally, the proposed calibrated model parameter settings obtained with Nodeworks UQ software were superior to the default MFiX-PIC settings and the settings proposed in the V&V Manual (Figure 24).

There were notable differences between the results obtained by PSUADE and Nodeworks (see Table 5). A comparison between PSUADE and Nodeworks-based calibrated model settings was then performed using the % relative error histogram method. As shown in Figure 25, PSUADE-based calibrated settings appear to give slightly more accurate results than Nodeworks-based calibrated settings for the location of filling shock ($y2$).

Finally, Table 6 shows the proposed calibrated settings for MFiX-PIC model parameters suggested for use in applications similar to the particle settling case. Although PSUADE-based results have been demonstrated to give more accurate MFiX-PIC simulation results, both settings could be used for applications that fall within the particle settling region of the hypothetical flow regime map shown in Figure 2.

A separate dedicated report will demonstrate statistical calibration for the settling case, which will yield distributions for the model parameter settings rather than single values. Then, additional standalone reports will describe the calibration efforts for the fluidized bed and circulating fluidized bed applications. The overall goal of these reports is to establish validated guidance for MFiX-PIC users who are planning to carry out simulations that fall within the hypothetical flow regimes explored while also offering a unified set of proposed calibrated settings.

Table 6: Validated Calibrated Model Parameters based on PSUADE and Nodeworks Results

MFiX-PIC Model Parameter	PSUADE Calibrated Settings for All ($\theta_1,\theta_2,\theta_3,\theta_4,\theta_5$)	Nodeworks Calibrated Settings for All ($\theta_1,\theta_2,\theta_3,\theta_4,\theta_5$)
Theta1 (θ_1): Pressure linear scale factor	**14.309**	**18.300**
Theta2 (θ_2): Vol. fraction exponential scale factor	**2.165**	**3.590**
Theta3 (θ_3): Statistical weight	**12.241**	**7.980**
Theta4 (θ_4): Vol. fraction at maximum packing	**0.399**	**0.442**
Theta5 (θ_5): Solid slip velocity factor	**0.828**	**0.658**

6. REFERENCES

Adams, B. M.; Hough, P. D.; Swiler, L. P. *Dakota Software Training: Model Calibration*; Technical Report; Sandia National Lab.(SNL-NM), Albuquerque, NM, 2015.

Andrews, M.; Snider, D. The multiphase particle-in-cell (MP-PIC) method for dense particulate flows. *International Journal of Multiphase Flow* **1995,** *22*, 379–402.

Auzerais, F.; Jackson, R.; Russel, W. The resolution of shocks and the effects of compressible sediments in transient settling. *Journal of Fluid Mechanics* **1988,** *195*, 437–462.

Banerjee, S.; Guenther, C.; Rogers, W. A. *Validating the MFiX-DEM Model for Flow Regime Prediction in a 3D Spouted Bed*; NETL-PUB-21381; NETL TRS Report, 2018.

Clarke, M.; Musser, J. *The MFiX Particle-in-Cell Method (MFiX-PIC) Theory Guide*; DOE/NETL-2020/2115; NETL Technical Report Series; U.S. Department of Energy, National Energy Technology Laboratory: Morgantown, WV, 2020; p. 28. DOI: 10.2172/1630414.

Desmond, K. W.; Weeks, E. R. Influence of particle size distribution on random close packing of spheres. *Phys. Rev. E* **2014,** *90*, 022204.

Dexter, W.; Tanner, D. Packing densities of mixtures of spheres with log-normal size distributions. *Nature Physical Science* **1972,** *238*, 31–32.

Gel, A.; Garg, R.; Tong, C.; Shahnam, M.; Guenther, C. Applying uncertainty quantification to multiphase flow computational fluid dynamics. *Powder Technology* **2013a,** *242*, 27–39.

Gel, A.; Li, T.; Gopalan, B.; Shahnam, M.; Syamlal, M. Validation and uncertainty quantification of a multiphase computational fluid dynamics model. *Industrial & Engineering Chemistry Research* **2013b,** *52*, 11424–11435.

Gel, A.; Vaidheeswaran, A.; Musser, J.; Tong, C. H. Toward the development of a verification, validation, and uncertainty quantification framework for granular and multiphase flows part 1: Screening study and sensitivity analysis. *Journal of Verification, Validation and Uncertainty Quantification* **2018,** *3*.

Gel, A.; Shahnam, M.; Musser, J.; Subramaniyan, A. K.; Dietiker, J.-F. Nonintrusive uncertainty quantification of computational fluid dynamics simulations of a bench-scale fluidized-bed gasifier *Industrial & Engineering Chemistry Research* **2016,** *55*, 12477–12490.

Heinrich, J.; Weiskopf, D. State of the Art of Parallel Coordinates. In *Eurographics (STARs)*; 2013; pp 95–116.

Iooss, B.; Lemaître, P. A review on global sensitivity analysis methods. In *Uncertainty management in simulation-optimization of complex systems*; Springer, 2015; pp 101–122.

Lu, L.; Benyahia, S. Advances in coarse discrete particle methods with industrial applications. *Advances in Chemical Engineering* **2018,** *53*, 53–151.

Musser, J.; Vaidheeswaran, A.; Clarke, M. *MFiX Documentation Volume 3: Verification and Validation Manual Second Edition*; NETL TRS Report; U.S. Department of Energy, National Energy Technology Laboratory: Morgantown, WV, 2018.

NETL. Nodeworks. National Energy Technology Laboratory, 2020. **https://mfix.netl.doe.gov/nodeworks**.

NETL. MFIX Solver Suite Documentation. **https://mfix.netl.doe.gov/mfix/mfixdocumentation/**. (accessed Jan 28, 2021).

Snider, D. Three dimensional multiphase particle-in-cell model for dense particle flows. *Journal of Computational Physics* **2001,** *170*, 523–549.

Snider, D. Three fundamental granular flow experiments and CPFD predictions. *Powder Technology* **2007,** *176*, 36–46.

Snider, D.; Clark, S.; O'Rourke, P. Eulerian-Lagrangian method for threedimensional thermal reacting flow with application to coal gasifiers. *Chemical Engineering Science* **2011,** *66*, 1285–1295.

Sobol, I. M. Global sensitivity indices for nonlinear mathematical models and their monte carlo estimates. *Mathematics and computers in simulation* **2001,** *55*, 271–280.

Thies-Weesie, D. M.; Philipse, A. P. Liquid permeation of bidisperse colloidal hard-sphere packings and the kozeny-carman scaling relation. *Journal of Colloid and Interface Science* **1994,** *162*, 470 – 480.

Tong, C. Problem Solving Environment for Uncertainty Analysis and Design Exploration, Version 01, 2010. **https://www.osti.gov//servlets/purl/1325009.**

Tong, C. Problem Solving environment for Uncertainty Analysis and Design Exploration (PSUADE). **https: //computing.llnl.gov/projects/psuade/software** (accessed Aug 2020).

Trucano, T. G.; Swiler, L. P.; Igusa, T.; Oberkampf, W. L.; Pilch, M. Calibration, validation, and sensitivity analysis: What's what. *Reliability Engineering & System Safety* **2006,** *91*, 1331–1357.

Vaidheeswaran, A.; Gel, A.; Clarke, M. A.; Rogers, W. A. *Sensitivity Analysis of Particle-In-Cell Modeling Parameters in Settling Bed, Bubbling Fluidized Bed and Circulating Fluidized Bed*; DOE.NETL-2021.2642; NETL Technical Report Series; U.S. Department of Energy, National Energy Technology Laboratory: Morgantown, WV, 2021; p 40. DOE: 10.2172/1756845.

Vaidheeswaran, A.; Musser, J.; Clarke, M. A. *Verification and Validation of MFiX-PIC*; NETL-TRS-2-2020; NETL Technical Report Series; U.S. Department of Energy, National Energy Technology Laboratory: Morgantown, WV, 2020; p. 48. DOI: 10.2172/1618293.

Viana, F. A. Things you wanted to know about the Latin hypercube design and were afraid to ask. In *10th World Congress on Structural and Multidisciplinary Optimization*; 2013.

Weber, J.; Fullmer, W.; Gel, A.; Musser, J. Optimization of a cyclone using multiphase flow computational fluid dynamics. *Journal of Fluids Engineering* **2020**, *142*.

APPENDIX

The purpose of this Appendix is to provide information necessary for the reader to reproduce the results of this report. There is expectation that the reader already has software access, as well as the necessary skill to work within and analyze results from associate software.

The files discussed in this section are available through NETL's Gitlab repository under the following URL:

https://mfix.netl.doe.gov/gitlab/quality-assurance/PIC_calibration/-/tree/main/Case1_ParticleSettling/DeterministicCalibration

All new users will need to register to gain access to the NETL Gitlab repository.

Registered users can clone the repository for all PIC Calibration related studies with the following git clone command from a Linux console terminal, then navigate to the folder where Deterministic Calibration related files reside:

```
1> git clone https://mfix.netl.doe.gov/gitlab/quality-assurance/PIC_calibration.git
2> cd PIC_calibration/Case1_ParticleSettling/DeterministicCalibration
```

For those who use a GUI based Git client, users can point to **https://mfix.netl.doe.gov/gitlab/quality-assurance/PIC_calibration.git** and clone the repository to their local system.

A directory tree is shown in the file README.md which provides an overview of the organization of the directories and stored files within this repository. For the remainder of the Appendix, the operating system level command examples displayed assume the bash shell environment. The reader should check their shell environment with "echo $SHELL" and make any necessary adjustments.

All files were tested in a MacOS based environment and are expected to be compatible with other operating system environments. If problems are experienced, the reader is encouraged to report them to the lead author via e-mail at aike@alpemi.com. Any other suggestions to improve the quality of the presented files and instructions in the appendix will be appreciated.

This page intentionally left blank.

APPENDIX A: INPUT FILES USED FOR PSUADE

All PSUADE analyses were performed with version 2.0. It is assumed that the user has setup their environment and path to the PSUADE 2.0 binary properly.

A.1. Importing External Dataset to PSUADE

List of the files used with hyperlinks to the repository:

SIM_Results_OLH_n120_i6_o3.xlsx : Microsoft® Excel file with the simulation dataset

OLH_n120_i6_o1_y2.dat : ASCII file with 120 samples with 6 input and 1 QoI

psData_OLH_n120_i6_o1_y2 : PSUADE native datafile generated after importing above file

Brief description of the files used:

PSUADE requires an input file with PSUADE command syntax, in addition to an actual dataset, to perform any type of analysis. The default filename for this file is psuadeData. The reader is strongly advised to use another name, like psData, as PSUADE will overwrite psuadeData without warning.

Typically, simulation campaign results are compiled in tabular format. The first several columns represent input parameters from the design of experiments, and the remaining columns report the associated quantities of interest. Each row represents a single sample from a simulation campaign. Figure A1 shows a screenshot of the first 40 rows of data from one of the simulation campaigns in this report. These were tabulated in Microsoft® Excel in preparation for analysis in PSUADE. This Microsoft® Excel file is saved in the repository under "SIM_Results_OLH_n120_i6_o3.xlsx", which is accessible at:

https://mfix.netl.doe.gov/gitlab/quality-assurance/PIC_calibration/-/blob/main/Case1_ParticleSettling/DeterministicCalibration/SIM_Results_OLH_n120_i6_o3.xlsx.

	q_1	q2	q_3	q_4	q_5	X1	Y1	Y2	Y3
MFiX-PIC Simulation Number	Emp.Pres. Constant	I. Fraction E Scale Facto	Stat.r Weight	Void Fraction at max packing	Velfac_Coeff	Initial Concentration	Location of settling shock	Location of filling shock	Void fraction at the first cell
1	4.375	**2.965**	4.388	0.478	**0.707**	**0.243**	**0.676**	**0.103**	**0.479**
2	17.049	**2.182**	6.917	0.441	**0.614**	**0.246**	**0.691**	**0.084**	**0.449**
3	3.860	**2.817**	8.729	0.368	**0.761**	**0.128**	**0.575**	**0.067**	**0.408**
4	19.782	**3.462**	16.329	0.418	**0.917**	**0.079**	**0.519**	**0.047**	**0.452**
5	1.572	**2.662**	18.853	0.495	**0.830**	**0.098**	**0.571**	**0.057**	**0.513**
6	9.356	**4.811**	3.246	0.472	**0.625**	**0.106**	**0.525**	**0.064**	**0.473**
7	4.613	**3.656**	19.361	0.363	**0.990**	**0.173**	**0.595**	**0.079**	**0.403**
8	8.892	**2.695**	14.690	0.372	**0.856**	**0.136**	**0.578**	**0.067**	**0.422**
9	15.462	**4.566**	19.936	0.407	**0.818**	**0.075**	**0.532**	**0.041**	**0.451**
10	9.795	**4.642**	6.737	0.424	**1.000**	**0.130**	**0.543**	**0.074**	**0.426**
11	14.360	**3.700**	18.536	0.489	**0.636**	**0.089**	**0.588**	**0.047**	**0.494**
12	3.531	**3.157**	15.467	0.480	**0.611**	**0.074**	**0.535**	**0.045**	**0.481**
13	18.016	**3.374**	5.465	0.373	**0.541**	**0.157**	**0.616**	**0.067**	**0.406**
14	3.201	**3.244**	12.546	0.406	**0.956**	**0.107**	**0.540**	**0.059**	**0.430**
15	11.773	**2.120**	16.688	0.470	**0.732**	**0.132**	**0.603**	**0.070**	**0.473**
16	17.773	**4.197**	10.865	0.497	**0.575**	**0.061**	**0.478**	**0.045**	**0.502**
17	12.139	**3.181**	17.799	0.350	**0.803**	**0.154**	**0.597**	**0.073**	**0.412**
18	10.386	**2.243**	18.177	0.397	**0.527**	**0.179**	**0.686**	**0.056**	**0.419**
19	6.361	**4.267**	8.992	0.395	**0.640**	**0.137**	**0.593**	**0.068**	**0.416**
20	1.927	**4.594**	4.961	0.486	**0.586**	**0.167**	**0.624**	**0.079**	**0.487**
21	7.923	**3.308**	17.454	0.433	**0.579**	**0.095**	**0.579**	**0.051**	**0.449**
22	13.928	**4.625**	15.328	0.359	**0.882**	**0.244**	**0.659**	**0.089**	**0.369**
23	2.432	**4.554**	13.349	0.429	**0.728**	**0.239**	**0.686**	**0.083**	**0.431**
24	10.716	**3.062**	6.490	0.360	**0.655**	**0.084**	**0.502**	**0.047**	**0.405**
25	15.648	**2.557**	6.035	0.490	**0.771**	**0.110**	**0.542**	**0.076**	**0.493**
26	1.282	**3.708**	10.969	0.458	**0.780**	**0.198**	**0.645**	**0.085**	**0.458**
27	3.034	**4.347**	18.420	0.474	**0.691**	**0.183**	**0.685**	**0.065**	**0.478**
28	14.002	**4.521**	5.618	0.457	**0.798**	**0.053**	**0.459**	**0.038**	**0.466**

29	6.734	**2.274**	3.743	0.435	**0.878**	**0.102**	**0.526**	**0.063**	**0.439**
30	6.781	**4.125**	18.047	0.377	**0.891**	**0.111**	**0.570**	**0.062**	**0.428**
31	14.277	**2.025**	7.665	0.376	**0.850**	**0.190**	**0.620**	**0.089**	**0.392**
32	15.903	**3.078**	16.156	0.493	**0.519**	**0.219**	**0.725**	**0.066**	**0.500**
33	17.346	**2.876**	19.556	0.459	**0.921**	**0.126**	**0.565**	**0.068**	**0.438**
34	19.639	**4.896**	12.084	0.378	**0.711**	**0.170**	**0.625**	**0.074**	**0.403**
35	18.600	**4.322**	4.181	0.444	**0.751**	**0.152**	**0.587**	**0.080**	**0.446**
36	10.571	**4.975**	14.150	0.495	**0.943**	**0.157**	**0.583**	**0.082**	**0.446**
37	12.609	**2.867**	3.183	0.431	**0.576**	**0.174**	**0.613**	**0.084**	**0.437**
38	0.488	**3.294**	7.583	0.382	**0.737**	**0.212**	**0.640**	**0.079**	**0.385**
39	5.184	**3.023**	14.355	0.390	**0.717**	**0.058**	**0.493**	**0.039**	**0.438**
40	0.563	**4.171**	15.091	0.450	**0.967**	**0.144**	**0.571**	**0.073**	**0.429**

Figure A1: First 40 samples of the tabulated dataset obtained from simulation campaign with 120 samples for 6 input parameters and 3 quantities of interest.

Figure A2 shows the first 34 lines of an ASCII formatted file, which is generated from the tabulated results shown in Figure A3. Note that the ASCII file contains an additional header line which indicates that 120 samples of the simulation campaign are included for 6 input parameters and 1 output (i.e., only second quantity of interest, y_2: Location of filling shock). This file is then imported into PSUADE. This particular ASCII file is saved in the repository under "OLH_n120_i6_o1_y2.dat," which is accessible at:

https://mfix.netl.doe.gov/gitlab/quality-assurance/PIC_calibration/-/blob/main/Case1_ParticleSettling/DeterministicCalibration/PSUADE/OLH_n120_i6_o1_y2.dat

```
120 6 1
4.375357683     2.964831514     4.388325271     0.477595333     0.707410724     0.242731915     0.103
17.04948779     2.181903742     6.917369989     0.440620168     0.614125616     0.245726825     0.0838
3.859943407     2.816860216     8.728581333     0.368275537     0.760834022     0.12829735      0.0666
19.78218578     3.462019191     16.32904762     0.418162837     0.91666567      0.078585083     0.0466
1.571820919     2.662006928     18.85345197     0.494644162     0.830245259     0.098355189     0.0566
9.356449166     4.811469404     3.246063344     0.471599941     0.624799244     0.106311291     0.0638
4.612861865     3.656385357     19.36074344     0.362722676     0.989536936     0.172857447     0.0794
8.891977257     2.69502557      14.68993561     0.372481687     0.855742809     0.135536976     0.067
15.46244199     4.565814093     19.93595151     0.40718106      0.818438893     0.075188818     0.0406
9.794747712     4.641684806     6.736548827     0.423840111     0.999860004     0.130339228     0.0742
14.36017168     3.699969307     18.53572717     0.488522566     0.635634662     0.088835674     0.0466
3.531403367     3.156698877     15.46732315     0.480034599     0.611236662     0.073909721     0.0446
18.01630693     3.374335595     5.465025422     0.373461983     0.540604339     0.156788699     0.067
3.201463522     3.244102794     12.54599382     0.405760859     0.956459093     0.106894208     0.0594
11.77287787     2.119800432     16.68819097     0.469760835     0.731597922     0.132497703     0.0702
17.77328513     4.196866131     10.86531528     0.49663611      0.574873687     0.060764722     0.0454
12.1392629      3.180670747     17.79894951     0.350158435     0.802848237     0.154070253     0.0726
10.38615417     2.243132312     18.17720191     0.396977772     0.527036637     0.178915452     0.0558
6.360520197     4.267258455     8.992355454     0.395484906     0.639868263     0.136913012     0.0678
1.927381721     4.594382542     4.961318484     0.48638239      0.585838499     0.166639357     0.0794
7.923091414     3.308081111     17.45396051     0.433156054     0.579349866     0.094832094     0.0506
13.9280133      4.624707803     15.32798043     0.358789633     0.882369886     0.244224507     0.0886
2.432124704     4.553522076     13.34861706     0.429376855     0.728426344     0.238740606     0.083
10.71613316     3.062482322     6.490146679     0.360101668     0.654995559     0.083976064     0.047
15.64813888     2.55691012      6.035243729     0.490355973     0.770528526     0.109692876     0.0758
1.282212596     3.708019758     10.96905479     0.458156748     0.78031981      0.198416687     0.0846
3.034284718     4.347128613     18.41969946     0.473553249     0.691058208     0.18296808      0.0646
14.00173707     4.521222911     5.617950257     0.45735116      0.797935655     0.052501381     0.0378
6.73440067      2.273516165     3.743382937     0.435150336     0.877770781     0.102451047     0.0634
6.780780542     4.125000841     18.04727098     0.37725787      0.890977021     0.11051259      0.0618
14.27672575     2.024661836     7.665202622     0.376071516     0.849778994     0.189982158     0.0886
15.90304356     3.07823418      16.15619454     0.493149318     0.519156369     0.218727644     0.0658
17.34636583     2.875559165     19.55579419     0.459422671     0.921452282     0.125725561     0.0678
"OLH_n120_i6_o1_y2.dat" line 1 of 121 --0%-- col 1
```

Figure A2: First 34 lines of the tabulated dataset obtained from simulation campaign with 120 samples for 6 input parameters and 3 quantities of interest. Grey colored numbers show the line number.

The contents of the simulation campaign dataset (`OLH_n120_i6_o1_y2.dat`) can be imported into PSUADE with the `read_std` command while running PSUADE interactively in command line mode. Details on how to import an ASCII file can be found in the PSUADE 1.7 Reference Manual (page 3).

Figure A3 shows the header segment of the imported file. Note that the ASCII header line used to indicate the number of samples in the simulation campaign, 6 input parameters and 1 output, has now been reformatted into a PSUADE native file format. This PSUADE native data file is saved in the repository under ”`psData_OLH_n120_i6_o1_y2`” , which is accessible at:

https://mfix.netl.doe.gov/gitlab/quality-assurance/PIC_calibration/-/blob/main/Case1_ParticleSettling/DeterministicCalibration/PSUADE/psData_OLH_n120_i6_o1_y2.

```
PSUADE_IO (Note : inputs not true inputs if pdf ~=U)
6 1 120
1 1
  4.3753576829999998e+00
  2.9648315140000001e+00
  4.3883252710000002e+00
  4.7759533300000001e-01
  7.0741072400000005e-01
  2.4273191499999999e-01
  1.0299999999999999e-01
2 1
  1.7049487790000001e+01
  2.1819037419999998e+00
  6.9173699890000000e+00
  4.4062016799999998e-01
  6.1412561600000004e-01
  2.4572682500000001e-01
  8.3799999999999999e-02
3 1
  3.8599434069999998e+00
  2.8168602159999998e+00
  8.7285813329999993e+00
  3.6827553699999999e-01
  7.6083402200000005e-01
  1.2829735000000000e-01
  6.6600000000000006e-02
4 1
  1.9782185779999999e+01
  3.4620191910000000e+00
  1.6329047620000001e+01
  4.1816283700000001e-01
  9.1666566999999999e-01
  7.8585083000000000e-02
  4.6600000000000003e-02
```

Figure A3: First 34 lines of PSUADE's native input file psData_OLH_n120_i6_o1_y2 obtained after importing the dataset in OLH_n120_i6_o1_y2.dat.

It is important to note that by default PSUADE will generate the psData_OLH_n120_i6_o1_y2 file with an INPUT section showing x1,x2,x3,… as the name of the input parameters, and y1,y2, y3,… as the names of the quantities of interest. It is recommended that the user edit psData_OLH_n120_i6_o1_y2 and rename the input and QoI parameters to indicate their values more appropriately. For example, in Figure A4, on line 967, x1 has been renamed t1:P_0, and on line 990, y1 has been renamed y2:LocFilling).

```
961   2.2858656799999999e-01
962   1.0140000000000000e-01
963 PSUADE_IO
964 PSUADE
965 INPUT
966    dimension = 6
967    variable 1 t1:P_0  =   4.8779439400000002e-01   2.0000224679999999e+01
968    variable 2 t2:beta  =   2.0000728950000002e+00   5.0000000000000000e+00
969    variable 3 t3:StatWeight  =   2.9636698739999998e+00   2.0007980220000000e+01
970    variable 4 t4:ep_gstar  =   3.5015843499999999e-01   4.9974982499999998e-01
971    variable 5 t5:VelfacCoeff  =   5.0113757199999998e-01   9.9986000399999997e-01
972    variable 6 x1:InitConc  =   5.0363092999999998e-02   2.4981387599999999e-01
973 #  PDF <inpNum> N  <mean> <std>
974 #  PDF <inpNum> L  <logmean> <std>
975 #  PDF <inpNum> T  <center> <halfbasewidth>
976 #  PDF <inpNum> B  <alpha> <beta>
977 #  PDF <inpNum> G  <alpha> <beta>
978 #  PDF <inpNum> W  <lambda> <K>
979 #  PDF <inpNum> IG <alpha> <beta>
980 #  PDF <inpNum> C  <X0> <gamma>
981 #  PDF <inpNum> E  <lambda>
982 #  PDF <inpNum> F  <D1> <D2>
983 #  PDF <inpNum> S  <filename> <index>
984 #  COR <inpNum> <inpNum> <value>
985 #  num_fixed = <count>
986 #  fixed <num> = <value>
987 END
988 OUTPUT
989    dimension = 1
990    variable 1 y2:LocFilling
991 END
992 METHOD
993    sampling = MC
994 #  sampling = FACT
```

Figure A4: The INPUT block of PSUADE native datafile (psData_OLH_n120_i6_o1_y2 lines: 961-994 shown) which shows the revised labels for input and output parameters.

A.2 SURROGATE MODEL CONSTRUCTION

List of the files used with hyperlinks to the repository:

PSbuildRS_2.in : PSUADE script file for batch mode surrogate model generation
R2_GPM10_120F_RSFA_CV_err.m : Cross-validation error assessment generated by PSUADE (the plot shown in Fig. 10)

Brief description of the files used:

Usually, PSUADE is run as an interactive session to facilitate the iterative analysis necessary to find the best data-fitted surrogate model. However, PSUADE can be invoked in batch mode by providing a script. Batch mode is best to automate tasks like construction of a response surface or cross-validation error assessment. Scripting requires that the user know exact syntax for each PSUADE command in order to construct a file that will work without user intervention.

Details on how to prepare such a script or how to interactively run PSUADE to test different surrogate models to find the best fit is beyond the scope of this Appendix. An example for such a script is saved in the repository under (PSbuildRS_2.in) which is accessible at:

https://mfix.netl.doe.gov/gitlab/quality-assurance/PIC_calibration/-/blob/main/Case1_ParticleSettling/DeterministicCalibration/PSUADE/1_ResponseSurface/GPM/PSbuildRS_2.in.

The script can be executed with the following command, where the output from PSUADE is redirected to a file named "run.log" for inspection:

```
1 > psuade PSbuildRS_2.in | tee run.log
```

Alternatively, the user can run PSUADE interactively and invoke the "rscheck" command. This method will require the user to provide responses to PSUADE queries related to different response surface model options, including set-up of a cross-validation error assessment.

A.3 SENSITIVITY ANALYSIS

List of the files used with hyperlinks to the repository:

matlabrssoboltsib.m : PSUADE output in Matlab format showing Total Sensitivity Indices (shown in Fig. 11)

Brief description of the files used:

Sensitivity analysis in PSUADE is performed after an adequate data-fitted surrogate model is constructed and its quality is established with an acceptable cross-validation error assessment outcome (see Figure 10). PSUADE offers multiple sensitivity analysis options. For a global sensitivity analysis, Sobol' indices method was chosen. Total indices were computed by issuing the command "rssoboltsib" during an interactive PSUADE session after the data file psData_OLH_n120_i6_o1_y2 was loaded. The user needs to respond to several questions to proceed, and depending on the bootstrapped sample size selected, it may take some time for PSUADE to finish the computations and generate a Matlab output file, matlabrssoboltsib.m.

Note that the output file will generate the plot shown in Figure 11.

A.4 DETERMINISTIC CALIBRATION

List of the files used with hyperlinks to the repository:

evalRSM_GPM10.c : Exported surrogate model from PSUADE in C language and revised for residual calculation during the evaluations required for optimization.

psuade.in : PSUADE script to perform the optimization loop to find the parameters that minimizes residual.

Exp_n21.dat : Experimental dataset used for guiding calibration process; the contents of this file are embedded in evalRSM_GPM10.c.

Brief description of the files used:

Deterministic calibration can be framed as an optimization problem which seeks to find the best settings for the 5 parameters under consideration that will result in a minimum residual (i.e., Simulation - Experiment). For the settling case presented in this report, experiments were replaced with an analytical solution for the quantity of interest. 21 samples were created by varying x_1: Initial solids concentration within the [0.05,0.25] interval. The file Exp_n21.dat shows the 21 samples generated in three columns: column 1 is x_1; column 2 is y_2^{exp}; and column 3, which is used to represent experimental uncertainty is empty (an analytical solution has no uncertainty). Instead of running full MFiX-PIC simulations, evaluations are performed with the surrogate model for given settings of $\theta_1,\theta_2,\theta_3,\theta_4,\theta_5$ and x_1. This evaluation is carried out by calling the evalRSM_GPM10 binary executable, which is built by compiling evalRSM_GPM10.c with the following command:

```
1 > gcc −o evalRSM_GPM10 evalRSM_GPM10.c −lm
```

Note that the above command assumes that the user has a working version of the GNU gcc compiler. evalRSM_GPM10.c is originally obtained from PSUADE by enabling the "rs_codegen" feature and constructing the surrogate model. The reader is referred to the PSUADE Manuals to learn how the command "rs_codegen" is used.

Once PSUADE exports the constructed surrogate model as a C-file, it should be renamed evalRSM_GPM10.c. Then, small modifications must be made. First, experimental data is incorporated directly into the code (lines 24–46). Then, the formulation for y should be modified from a calculation for the QoI to the calculation of residual between the experimental data and the analytical solution (lines 76–78). The user can identify and better understand the changes implemented by comparing the evalRSM_GPM10.c file in the repository to the original exported surrogate model for the same dataset and same type of surrogate model.

To run the optimization procedure and save the output coming to the screen, the following command is issued:

```
1 > psuade psuade.in | tee run.log
```

After successful execution, PSUADE will report the best solution under the PSUADE OPTIMIZATION : CURRENT GLOBAL MINIMUM heading. For best results, extract the output of each trial, then visualize with a parallel coordinates plot to observe convergence trends over multiple attempts.

APPENDIX B: INPUT FILES USED FOR NODEWORKS

All of the analyses performed with Nodeworks were carried out with version 20.1.1. For success, the conda environment and all dependent Python libraries must be installed properly. It is strongly recommended to check the node libraries installed at the beginning of a Nodeworks session by selecting the leftmost icon on the top row of Show Main Menu, and then clicking on the Node Library menu item as shown in Figure B1.

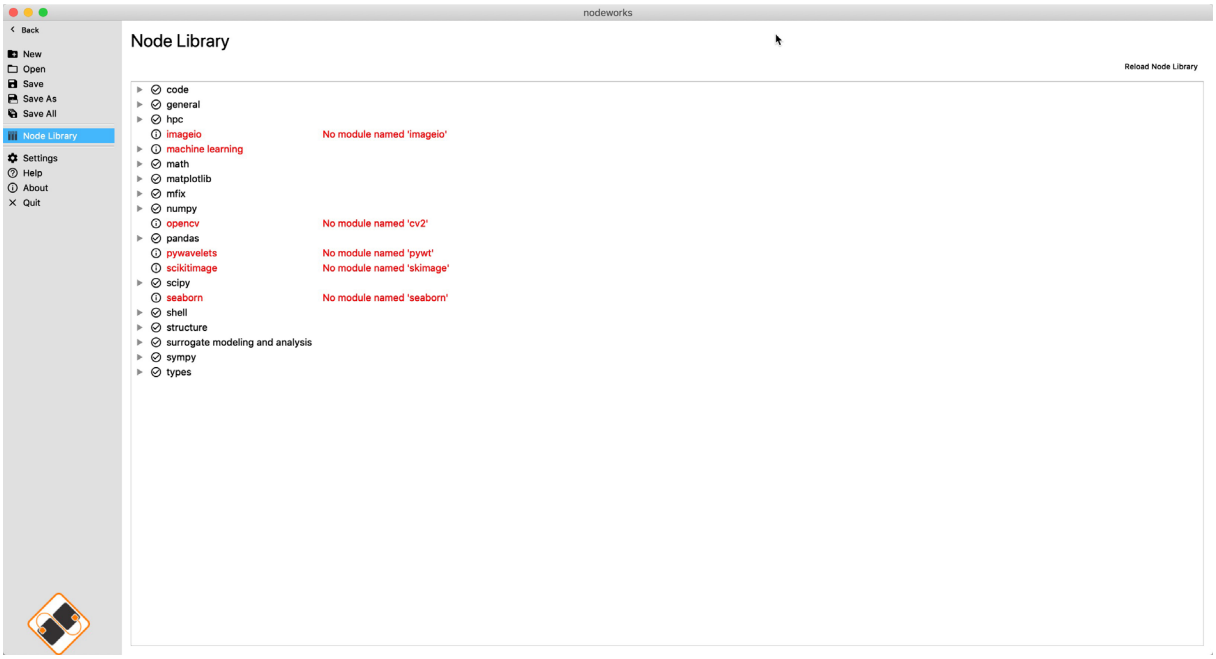

Figure B1: Screenshot of libraries loaded at the beginning of Nodeworks session under Show Main Menu.

List of the files used with hyperlinks to the repository:

OLH_n120_i6_o1.csv : CSV formatted input file which contains the simulation campaign results and is imported into Nodeworks through Response Surface node. exp_n21.csv : CSV formatted experimental dataset used for guiding calibration process; the contents of this file imported into Residual Function node.

SIM_n120_Calibration.nc : Nodeworks worksheet containing the group of nodes compiled to perform deterministic calibration workflow.

Brief description of the files used:

SIM_n120_Calibration.nc contains the workflow constructed in Nodeworks to perform the deterministic calibration. First, a surrogate model for the imported dataset (OLH_n120_i6_o1.csv) is constructed. Then, optimization is performed in the General Optimizer node by finding the combination of $\theta_1,\theta_2,\theta_3,\theta_4,\theta_5$ settings that yield the lowest residual (computed in the Residual Function node). The experimental dataset (in this case, the 21 samples of analytical solution) is

introduced to the workflow by importing `exp_n21.csv` into the Residual Function node. The user may need to change some settings in the General Optimizer, such as the number of attempts to perform the optimization. It may also be necessary to change convergence tolerances. Once the workflow is executed (by hitting the Play button), the results of the optimization can be visualized in the Parallel Coordinates plot tab.

Brian Anderson
Director
National Energy Technology Laboratory
U.S. Department of Energy

John Wimer
Associate Director
Strategic Planning
Science & Technology Strategic Plans & Programs
National Energy Technology Laboratory
U.S. Department of Energy

Traci Rodosta
Strategic Planning
Science & Technology Strategic Plans & Programs
National Energy Technology Laboratory
U.S. Department of Energy

Mark Ackiewicz
Director
Division of Carbon Capture and Storage
Office of Fossil Energy
U.S. Department of Energy

Bryan Morreale
Executive Director
Research & Innovation Center
National Energy Technology Laboratory
U.S. Department of Energy